Ore Geology Reviews 89 (2017) 390–406

Contents lists available at ScienceDirect

Ore Geology Reviews

journal homepage: www.elsevier.com/locate/oregeo

# Geochemistry of Archean Radioactive Quartz Pebble Conglomerates and Quartzites from western margin of Singhbhum-Orissa Craton, eastern India: Implications on Paleo-weathering, provenance and tectonic setting

Ajay Kumar [a,*], A.S. Venkatesh [b], Pramod Kumar [a], A.K. Rai [c], P.S. Parihar [c]

[a] Atomic Minerals Directorate for Exploration and Research, Jamshedpur 831002, India
[b] Indian Institute of Technology (Indian School of Mines), Dhanbad 826004, India
[c] Atomic Minerals Directorate for Exploration and Research, Hyderabad 500016, India

ARTICLE INFO

*Article history:*
Received 3 October 2016
Received in revised form 3 June 2017
Accepted 10 June 2017
Available online 12 June 2017

*Keywords:*
Radioactive Quartz Pebble Conglomerate
Quartzite
Paleo-weathering, Provenance
Tectonic implications
Eastern India

ABSTRACT

Lenses of radioactive Quartz Pebble Conglomerates (QPC) and associated quartzites are exposed along western margin of Archean Bonai Granite in Singhbhum-Orissa Craton, eastern India intermittently spreading over a strike length of 8–10 km. QPCs are radioactive while quartzites are mostly non-radioactive in nature. The purpose of the research is to investigate and characterize the radioactive QPC and quartzites geochemically to decipher their paleo-weathering conditions, provenance characteristics and possible tectonic setting of deposition. Geochemical data suggest moderate to high chemical weathering conditions in the provenance areas of QPC and quartzites. Major, trace and REE data indicate predominantly felsic to partly mafic-ultramafic sources for the deposition of radioactive Quartz Pebble Conglomerates from the surrounding Archean terrain.

Elevated values of Th, U, Pb, La, Ce, Y and low Sc with high critical trace elemental ratios of Th/Sc, La/Sc, Th/Cr and Zr/Sc in radioactive QPC indicate their derivation from felsic igneous source. Low concentration of Th and Sc in quartzites compared to QPC and their variable Th/Sc ratios indicate both felsic and mafic sources for quartzites, albeit their preferential felsic affiliation. Higher Cr/Th ratios in quartzites (18.4), moderate Cr/Th in QPC (5.42), low to moderate Y/Ni in QPC (0.36–12.4) and quartzite (0.29–1.88), along with Au ranging from 30 to 1527 ppb, Pt up to 188 ppb and 682 ppb in QPC and quartzites respectively point towards some contribution from mafic-ultramafic source as well. REE patterns and in particular negative Eu anomalies for both QPC and quartzites further support their derivation from felsic rocks and could possibly linked to some of the phases of Archean Singhbhum Granite and Bonai Granite. Granitic to pegmatitic source for QPC is also revealed by the presence of rounded to sub-rounded monazite, zircon and thorian-uraninite grains in their matrix. Study indicates that QPC and quartzites were deposited in a passive margin tectonic setting developed during Archean between a span of 3.3 and 3.16 Ga along the western margin of Bonai Granite when the reducing condition was prevalent as indicated by their low Th/U ratios (<4.0) and presence of detrital grains of uraninite and pyrite in QPC. Radioactive QPC from western margin of Archean Singhbhum-Orissa Craton bears broad resemblance with QPC from Witwatersrand basin of South Africa and Elliot Lake, Canada and thus appears to be ideal sites for exploring QPC hosted U (+Au-PGE) mineralization in the analogous areas.



## 1. Introduction

Archean Singhbhum-Orissa Craton (SOC) is one of the important mineral belts of India hosting deposits of Iron, Copper and gold (Saha, 1994; Mahadevan, 2002; Sahoo and Venkatesh, 2015). Vein type uranium mineralization is noted all along the younger Singhbhum Shear Zone (SSZ) while the other types of uranium mineralization finds are not economically exploited so far. The study area forms part of SOC where search for QPC-type mineralization has been initiated by Atomic Minerals Directorate for Exploration and Research (AMD) and met with significant success (Vasudeva Rao et al., 1988; Das et al., 1988; Mishra et al., 1997; Mishra et al., 2008; Kumar et al., 2011a,b, 2012). This is important both

* Corresponding author.
*E-mail address:* ajaykumar.amd@gov.in (A. Kumar).

http://dx.doi.org/10.1016/j.oregeorev.2017.06.014
0169-1368/

in terms of academic and economic point of view as the QPC-type uranium deposits share 13% of the total known uranium resources globally (Red Book, 2011; Dhalkamp, 1993) generally accompanied by gold, REE and PGE (Frimmel, 2005). Two such types of World class deposits occur in Witwatersrand Basin, South Africa (mainly Au- and U) and Blind River deposit (U-Y) in Elliot Lake, Canada (IAEA, 1996; Frimmel and Minter, 2002; Hazen et al., 2009). In India, QPC contribution is only 0.22% of all uranium resources of the country (Parihar, 2012).

It is well established that QPC hosted uranium deposits are found in Archean and Paleoproterozoic ages of rocks older than 2200 million years (Robertson, 1962; Schidlowski, 1975; Grandstaff, 1980, 1981; Smith and Minter, 1980; Robinson and Spooner, 1982; Saager and Stupp, 1983; Phillips and Law, 2000; Frimmel and Minter, 2002; Dankert and Hein, 2010; Bergen and Fayek, 2012 and Uvarova et al. 2014). Exploration in similar geological setups in India led to the discovery of uraniferous QPC at Walkunji in Dharwar Craton, Karnataka, south India (Rama Rao, 1974; Viswanath et al., 1988; Pandit, 2002). In eastern India, uranium and gold bearing basal conglomerates are traced in Dhanjori basin (Vasudeva Rao et al.,1988; Haque et al., 2001), Gorumahisani–Badampahar basin (Das et al., 1988), at the base of IOG in Koira-Noamundi basin (Mishra et al.,1997; Kumar, et al., 2009, 2011a,b, 2012), Daitari-Tomka basin (Mishra et al., 2008; Kumar, et al., 2011a) and in Mankharhachua basin (Chakrabarti et al., 2011). Mukhopadhyay et al. (2016) described the depositional control, nature and source of detrital uraninite from Mahagiri Quartzite in Daitari-Tomka basin. Ghosh et al. (2016) from a stratigraphically equivalent quartzite-conglomerate succession from the southern and central parts of the Singhbhum Craton reconstructed the provenance, tectonic setting and paleo-weathering conditions and nature of upper crust of the Singhbhum Craton.

Though preliminary exploration studies have been conducted in all these basins to locate QPC type uranium deposits, the detailed geochemical studies are limited from the western margin of Singhbhum-Orissa Craton especially in siliciclastic sequences deposited along the margin of Singhbhum Granite batholiths while Mukhopadhyay et al. (2016), Ghosh et al. (2016) conducted detailed studies on southern and central portions. In this paper, an attempt has been made to infer the provenance characterization, paleo-weathering conditions and possible tectonic setting of QPC-quartzite sequence deposited around Archean Bonai Granite in parts of Sundargarh district of Orissa, eastern India. The study is also aimed to evaluate the suitability of the basin for locating QPC hosted U (+Au-REE-PGE) mineralization based on field, petrographical and geochemical inputs in the adjoining areas.

## 2. Regional geological setup

The study area is included in survey of India toposheet No. 73 C/13 and is located north of Bonai town and south of Raghunathpalli and forms the western part of SOC of eastern India (Fig. 1). Mahalik (1987) grouped the rocks lying between Bonai Granite and Gangpur rocks into a new group designated as Darjing Group. The QPC- quartzite sequence is exposed between basal Bonai Granite and Darjing Group and extends over a strike length of 8–10 km intermittently between Baratangra in the west to Phuljhori Pahar in the east (Kumar et al., 2009). QPC-quartzite unit unconformably overlie Bonai Granite (3.16 Ga) and is underlain by Birtola Formation of Darjing Group (Mahalik, 1987) (Fig. 1). QPCs are younger than Bonai Granite is also evidenced from the absence of enclaves of QPCs within BG. The 2.8 Ga old Tamperkola Granite intruded the Bonai Granite (Bandyopadhyay et al., 2001). Thus, the age of the QPC-quartzite unit may be interpreted to be around 3.16–2.8 Ga. U–Pb LA-ICPMS ages from the western IOG acid volcanic rocks suggests an age of 3.29 Ga (Basu et al., 2008).

QPC are radioactive, while quartzites are mostly non-radioactive. Moderate to steeply dipping, current-bedded fuchsite-bearing quartzites (Fig. 2A) are associated with meta-volcanic rocks and at places exhibit cross bedding. The ferruginous quartzites occur at the contact zones of radioactive QPC and basal Bonai Granite (Fig. 2B & C). Thin lensoidal bodies of QPC interbedded with the quartzites are found near Birtola (Fig. 2D), 500 m east of Birtola village in Phuljhari Pahar. Bonai Granite is represented by migmatitic granite (phase-I) (Fig. 2E) occur as enclaves within porphyritic granite (Phase-II) (Fig. 2F). Oligomictic QPC occurs at the base of the litho package at Bagiyabahal. The quartzites are exposed in a series of hills extending from north of Darjing to south of Gurundia along the northwestern boundary of Bonai Granitic Pluton. Phase-I of Bonai Granite is 3369 ± 57 Ma and phase- II is 3163 ± 126 Ma old (Sengupta et al., 1991, 1996). According to Bandyopadhyay et al. (2001), the age of deposition and metamorphism of the Darjing Group metasediments overlying QPC- quartzite sequence falls between ~3.2 Ga and 2.8 Ga.

## 3. Occurrence of radioactive QPC

QPC are mostly inter-bedded with quartzites as small individual lensoidal bodies of varying dimensions and also at the base near Baratangra village and north of Balisura in Phuljhori Pahar. They trend NE-SW direction with moderate to steep dips varying from 53° to 85° towards NW (Fig. 1). QPCs are generally radioactive with substantial U and Th values and their Th/U ratios ranging from 1.56 to 3.86 (Kumar et al., 2009). QPC show presence of both white vein quartz as well as smoky quartz pebbles with stains of iron oxides (Fig. 2B). Graded bedding is also noted in QPC-quartzite sequence along the right bank of Brahmani river section where coarser pebbles in QPC occur at the base while finer pebbles occurs above the sequence, which finally grades into fine grained quartzites (Fig. 2C). QPCs are also well exposed around Bagiyabahal, near Birtola village along left bank of Brahmani river and at hill top in Phuljhori Pahar section. These QPCs were mapped on 1: 1000 scale to decipher their nature of disposition and their dimension (Kumar and Pande, 2005) with respect to quartzites and basal Bonai Granite (Fig. 1).

Sarkar and Saha (1992) equated these quartzite units bordering western fringe of BG with IOG rocks based on the aerial photo interpretation and similar tectonic trend. Ghosh et al. (2016) suggested that Keonjhar Quartzite lies unconformably above 3.1–3.4 Ga old Singhbhum Granite-II basement in the Singhbhum Craton. Mukhopadhyay et al. (2014) also suggested a Mesoarchean age of deposition (~3 Ga) for Keonjhar Quartzite based on detrital zircon ages, intrusive relationship with granites, and the presence of detrital minerals like uraninite and pyrite in them. Similar situation is also observed in the present study wherein QPC-quartzite unit overly basement Bonai Granite-II (3.16 Ga) intruded by 2.8 Ga old Tamperkola Granite (Bandyopadhyay et al., 2001). Based on this analogy, QPC-quartzite unit of study area is comparable with Mesoarchean Keonjhar Quartzite and Mahagiri Quartzite of Singhbum Craton (Mukhopadhyay et al. 2014; Ghosh et al., 2016).

## 4. Analytical methods

Twenty-one samples of QPC and fifteen samples of quartzites were selected for whole-rock and trace element analysis using a PANalytical Magi X Pro PW 2440 WDXRFS unit eqipped with a 4 Kw, 60 kV, 125 mA super sharp end window type X-ray tube at XRF Laboratory of AMD, DAE, Hyderabad. International standard reference materials (SRM's) viz., G-2, GA, GH, GS-N, JG2, MAN.

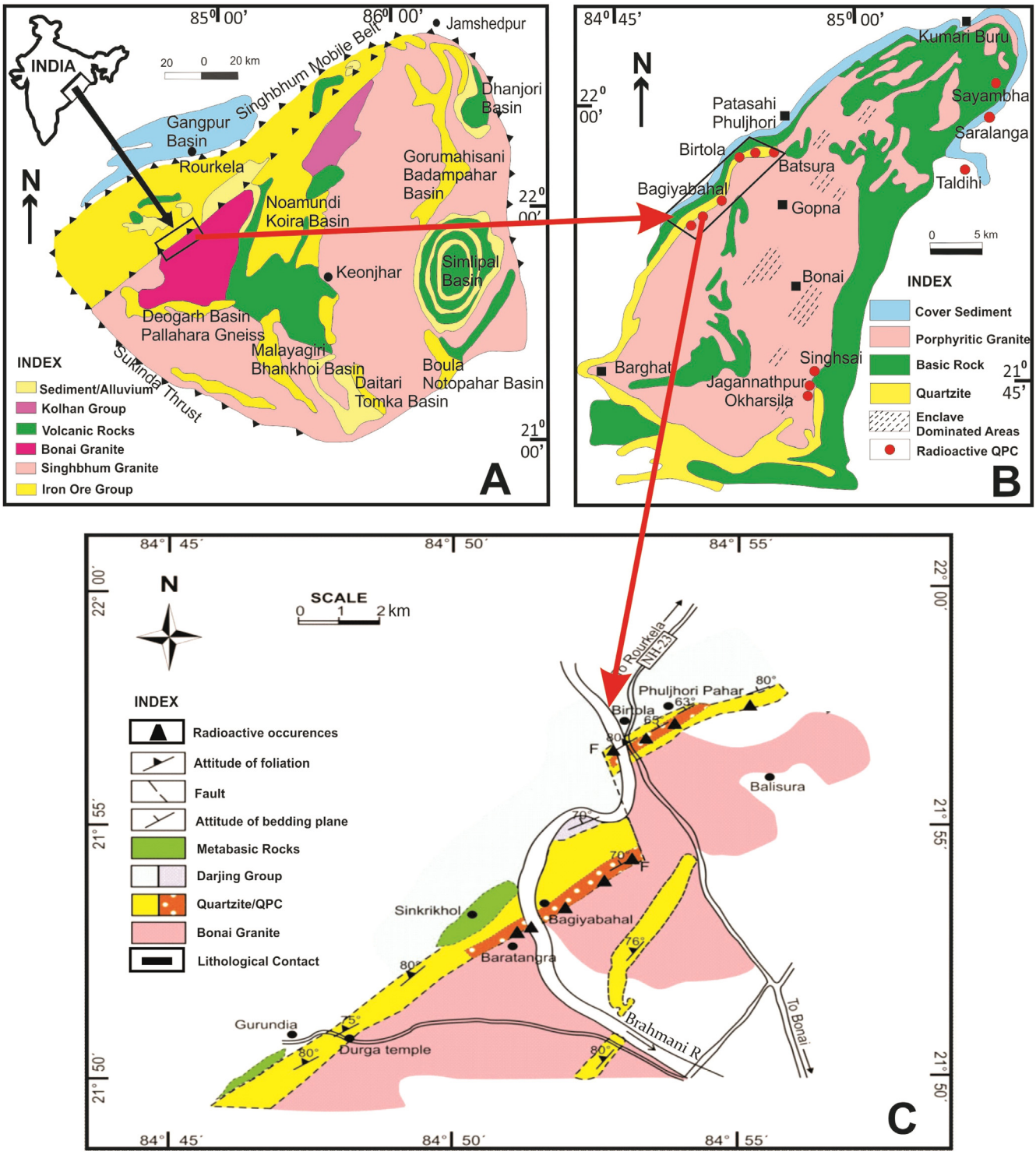


**Fig. 1.** Geological maps of study area: A) Geological map of Singhbum–Orissa Craton showing location of the study area. (Redrawn from Saha, 1994); B) Geological map showing important prospective radioactive QPC along the western fringe of Bonai Granite (after Sengupta et al., 1991); C) Geological map between Gurundia and Phuljhori Pahar, Sundargarh district, Orissa with a NNE-SSW trending QPC–Quartzite sequence dislocated by a major fault showing locations of radioactive QPC.

SG3, ACE JG-1a (all granites), JG-3, GSP-1 (granodiorite) etc. were used as calibration standards. The major and minor elements were analyzed at 30 kV and 100 mA using 300 m collimator, PX 1 and LIF 200 dispersing crystals and gas flow proportional counter detectors with detection limit of 0.01% whereas the trace elements were analyzed at 50 kV and 60 mA using 150 μm collimator, LIF 220 crystals and scintillation and/duplex detectors with detection limit of 10 ppm.

The analytical precision (% RSD) and accuracy (% error) was within ±5% for major elements, minor elements (>30 ppm) and ±10% for trace elements (<30 ppm). $Na_2O$ wt% in QPC was determined using flame photometry. Loss on ignition (LOI) and FeO in all samples were determined at Chemical Laboratory, AMD, Jamshedpur. Low total oxide content in a few samples could be due to high siliceous nature of rocks and due to non-determination of some elements like $Cr_2O_3$ by XRF and non-

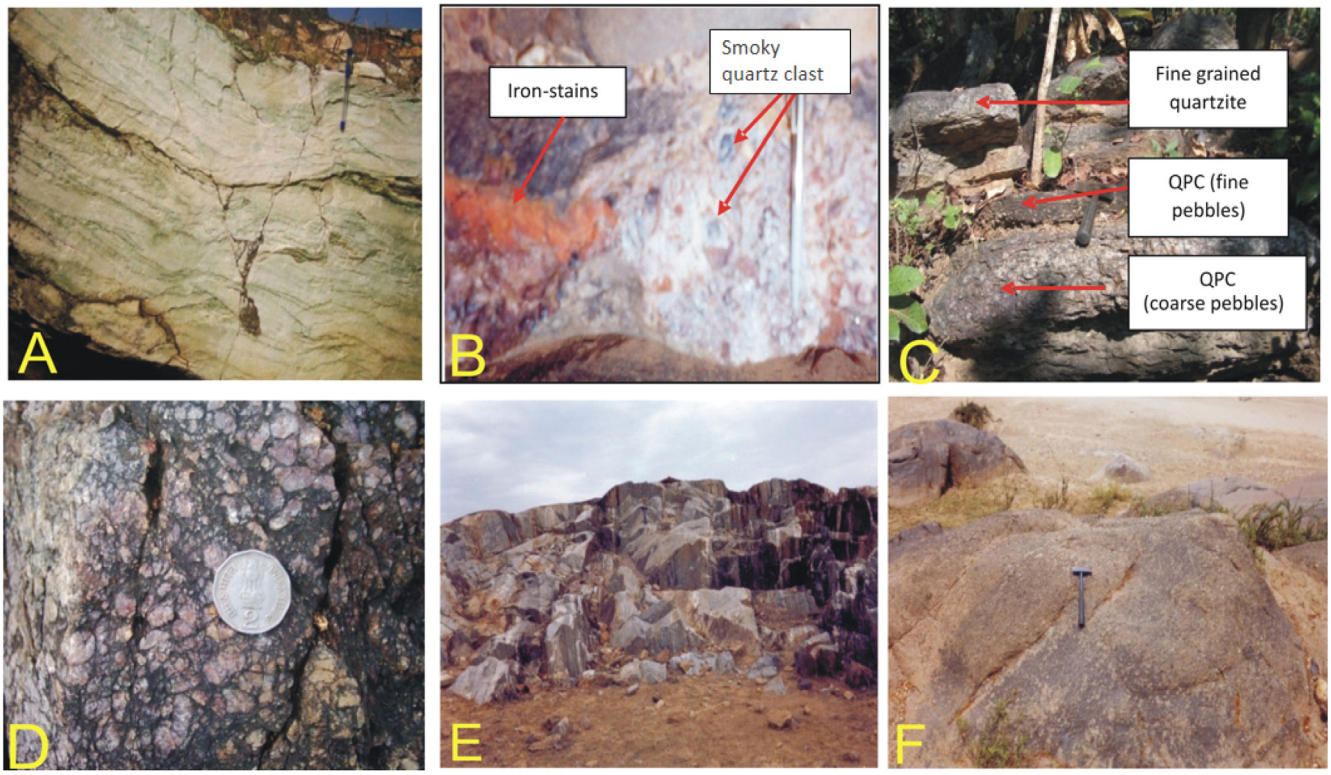


**Fig. 2.** Field relations of radioactive quartz pebble conglomerate lenses and quartzites; A) Outcrops of quartzite near Birtola village contain significant amounts of layered fuchsite suggesting possible involvement of Cr in the provenance; B) Occurrence of radioactive QPC along the right bank of Brahmani River in the western margin of Bonai Granite with ash grey colored smoky quartz pebbles; C). Radioactive QPC showing gradation from coarse grained pebbles to fine grained pebbles along the dip direction in the central part of Bagiyabahal area, western margin of Bonai Granite; D) Matrix supported radioactive QPC near Birtola village; E) Occurrence of Phase-I, migmatitic Bonai Granite, Bonaigarh; F) Outcrops of porphyritic, Phase-II Bonai Granite as seen 50 m south of Bagiyabahal village.

addition of $RE_2O_3$ in total which are significant in QPC and quartzites. Trace elements viz., Th, U, Sc, Hf and REE were determined using ICP-MS-Platform XS at Chemical Laboratory of AMD, DAE, Hyderabad and the standards used are SY-2, SY-4, and MRG-1. For different REE elements percentage error varies from 1.0 to 10. For U and Th, detection limit are 0.22 and 0.21 ppm respectively and the error in determination for both elements is 2%.

Five samples each of QPC and quartzites are considered for PGE analyses in view of their relatively higher concentration of gold. REE, Au and PGE were determined in the samples as per the procedure adopted after Lichte et al. (1987) and Oguri et al. (1999). Au was analyzed by pre-concentration with Tellurium (Te) and later determined using Graphite furnace AAS (Zeenit 650 of Analytika Jena) at Chemistry laboratory, AMD, Hyderabad with attached auto-sampler MPE 60 at wavelength of 242.8 nm. The above procedure is validated by analyzing Certified Reference Material (CRMs) {(MA-1b Au- 17 ppm), (SARM-53, Au 3.99 ppm)}. Instrument detection limit for Au is 4 ppb, detection limit for the method followed is 20 ppb and error percentage is 10%. Details regarding instruments used, make, model, determination limit, error, standards used for estimation of various elements were given in Kumar et al. (2011).

## 5. Geochemistry of QPC and quartzites

Geochemistry of sedimentary rocks can be used to infer source rock composition, weathering, transport history and depositional conditions of sedimentation (McLennan et al., 1993). Investigations on geochemical characteristics of ancient and modern sediments have been carried out by various workers to infer the source rocks, provenance and tectonic setting (Bhatia, 1983; Bhatia and Crook, 1986; Roser and Korsch, 1986, 1988; Nesbitt et al., 1996 followed by several workers). The major elemental geochemical parameters have been used to define tectonic settings of different sedimentary suites (Bhatia, 1983; Roser and Korsch, 1986).

Geochemistry of quartzite and radioactive QPC are analyzed to understand the inter-elemental variations to decipher the possible source characterization, evolution and metallogenetic implications (Tables 1–6). Comparison of major elemental ratios of QPC and quartzites are given in Tables 1 and 2. There are significant variations between these two types of rocks. Major oxides have been used by various workers for geochemical classification of terrigenous sediments (Pettijohn et al., 1972; Heron, 1988). In binary plot of log ($SiO_2/Al_2O_3$) vs log ($Na_2O/K_2O$) (Pettijohn et al., 1972), 50% of QPC samples fall in the field of arkose to sub-arkose and rest is plotted in sub-litharenite field. Most of the quartzites plot in arkose to sub-arkose field; three samples occupy the boundary of sub-arkose to sub-litharenite field (Fig. 3A). The ratio $Fe_2O_3/K_2O$ allows arkose to be more successfully classified and it is a measure of mineral stability (Nagarajan et al., 2007). Out of 21 samples of QPC, ten samples plot in sub-litharenite field, five samples in Fe-sands field whereas two samples each occupy the field of arkose, sub-arkose and quartz-arenite (Heron 1988). All the quartzites occupy sub-arkose field except one sample which plots in quartz-arenite field (Fig. 3B).

$TiO_2$ content in QPC ranges from 0.10 to 1.22 whereas in quartzite, it varies from 0.01–0.57, which may be due to the presence of more titanium bearing minerals in QPC such as rutile, ilmenite and anatase. Low $Al_2O_3/TiO_2$ ratios in QPC compared to quartzites (Tables 1 and 2) may indicate the presence of Ti- bearing mafic mineral phases like biotite, chlorite and ilmenite from a mixed source (Chakrabarti et al., 2009). $K_2O/Al_2O_3$ ratio for QPC ranges

**Table 1**
Geochemical data showing major oxide concentrations of QPC from the western margin of Singhbhum-Orissa Craton.

| Sample/Oxides (in wt%) | DP/8 | DP/81 | DP/86 | DP/90 | DP/23 | DP/2 | DP/14 | DP/28A | DP/35 | DP/55 | Bali/1 | Bali/8 | Bali/10 | BBL/41 | BBL/52 | BBL/70 | BBL/74 | BBL/78 | BBL/85 | BBL/90 | BBL/100 |
|---|---|---|---|---|---|---|---|---|---|---|---|---|---|---|---|---|---|---|---|---|---|
| $SiO_2$ | 86.35 | 93.45 | 86.89 | 91.75 | 85.32 | 92.6 | 84.94 | 92.39 | 87.88 | 90.23 | 86.33 | 92.96 | 93.13 | 96.36 | 88.42 | 95.3 | 92.17 | 96.73 | 92.25 | 90.48 | 90.9 |
| $TiO_2$ | 1.22 | 0.47 | 0.38 | 0.86 | 0.33 | 0.73 | 0.73 | 0.1 | 0.54 | 0.12 | 0.17 | 0.2 | 0.35 | 0.39 | 0.87 | 0.48 | 0.48 | 0.26 | 0.17 | 0.12 | 0.64 |
| $Al_2O_3$ | 4.83 | 1.45 | 2.1 | 2.14 | 7.56 | 2.01 | 7.2 | 2.16 | 5.39 | 3.74 | 4.92 | 2.31 | 1.74 | 1.51 | 4.19 | 2.88 | 3.9 | 2.26 | 4.12 | 4.14 | 4.12 |
| $Fe_2O_3$(t) | 1.79 | 5.25 | 2.75 | 4.8 | 1.11 | 3.28 | 1.57 | 1.69 | 1.55 | 2.21 | 3.65 | 4.15 | 3.24 | 1.43 | 1.76 | 1.39 | 1.12 | 1.11 | 1.03 | 1.64 | 2.31 |
| FeO | 0.58 | 1.72 | 1.36 | 2.44 | 0.58 | 1.21 | 0.64 | 1.08 | 1.22 | 1 | 0.79 | 1.08 | 1.08 | 1.08 | 0.58 | 0.64 | 0.5 | 0.64 | 0.72 | 0.72 | 1.24 |
| MnO | 0.01 | 0.02 | 0.01 | 0.01 | 0.01 | 0.03 | 0.04 | <0.01 | <0.01 | 0.01 | <0.01 | <0.01 | <0.01 | <0.01 | 0.01 | 0.01 | 0.01 | 0.01 | 0.02 | <0.01 | 0.01 |
| MgO | 0.47 | 0.45 | 0.52 | 0.81 | 0.2 | 1.41 | 0.36 | 0.39 | 0.65 | 1.26 | 0.13 | 0.26 | 0.06 | 0.25 | 0.04 | 0.23 | 0.11 | 0.21 | 0.11 | 0.09 | 0.57 |
| CaO | 0.04 | 0.04 | 0.02 | 0.04 | 0.01 | 0.04 | 0.01 | 0.01 | <0.01 | 0.05 | 0.02 | 0.03 | 0.04 | 0.01 | <0.01 | <0.01 | <0.01 | 0.01 | 0.01 | 0.01 | 0.03 |
| $Na_2O$ | 0.07 | 0.12 | 0.1 | 0.16 | 0.29 | 0.23 | 0.16 | 0.08 | 0.14 | 0.21 | 0.27 | 0.17 | 0.17 | 0.11 | 0.05 | 0.09 | 0.16 | 0.07 | 0.09 | 0.13 | 0.08 |
| $K_2O$ | 1.33 | 0.19 | 0.35 | 0.2 | 2.03 | 0.23 | 1.86 | 0.52 | 1.15 | 0.63 | 0.99 | 0.49 | 0.36 | 0.47 | 1.08 | 0.85 | 1.1 | 0.64 | 1.09 | 1.13 | 0.82 |
| $P_2O_5$ | 0.08 | 0.06 | 0.05 | 0.1 | 0.03 | 0.08 | 0.05 | 0.02 | 0.03 | 0.06 | 0.04 | 0.04 | 0.04 | 0.02 | 0.03 | 0.03 | 0.03 | 0.02 | 0.02 | 0.02 | 0.05 |
| LOI | 0.82 | 0.73 | 0.67 | 1.19 | 0.93 | 0.86 | 1.05 | 0.45 | 0.72 | 0.98 | 0.88 | 0.44 | 0.78 | 0.16 | 0.87 | 0.56 | 0.69 | 0.4 | 0.51 | 1.93 | 0.45 |
| Total | 97.59 | 103.95 | 95.2 | 104.5 | 98.3 | 102.71 | 98.61 | 98.89 | 99.27 | 100.5 | 98.19 | 102.13 | 100.99 | 101.79 | 97.9 | 102.46 | 100.27 | 102.36 | 100.14 | 100.41 | 101.22 |

**Table 2**
Geochemical data showing major oxide concentrations of quartzites from the western margin of Singhbhum-Orissa Craton.

| Sample/Oxides (in wt%) | AK/DP/5 | AK/DP/10 | AK/DP/11 | AK/DP/16 | AK/DP/20 | AK/DP/45 | AK/DP/54 | AK/DP/64 | AK/DP/73 | AK/DP/76 | AK/DP/89 | AK/BBL/12 | AK/BBL/47 | AK/BBL/59 | AK/BBL/66 |
|---|---|---|---|---|---|---|---|---|---|---|---|---|---|---|---|
| $SiO_2$ | 87.25 | 87.47 | 85.92 | 83.95 | 85.83 | 84.05 | 93.97 | 87.54 | 87.21 | 87.41 | 92.86 | 89.72 | 93.52 | 97.59 | 91.93 |
| $TiO_2$ | 0.29 | 0.18 | 0.29 | 0.57 | 0.19 | 0.2 | 0.01 | 0.13 | 0.27 | 0.04 | 0.04 | 0.08 | 0.2 | 0.15 | 0.18 |
| $Al_2O_3$ | 5.25 | 5.28 | 5.47 | 6.53 | 5.65 | 6.52 | 2.2 | 5.16 | 5.25 | 5.12 | 3.03 | 4.4 | 2.85 | 1.13 | 3.4 |
| $Fe_2O_3$(t) | 0.32 | 0.28 | 0.27 | 0.55 | 0.37 | 0.21 | 0.14 | 0.43 | 0.33 | 0.23 | 0.22 | 0.25 | 0.2 | 0.11 | 0.3 |
| FeO | 0.86 | 0.51 | 0.51 | 0.58 | 0.64 | 0.36 | 0.58 | 1.08 | 0.79 | 0.72 | 0.74 | 0.72 | 0.42 | 0.36 | 1.08 |
| MgO | 0.51 | 0.65 | 0.45 | 0.46 | 0.43 | 0.15 | 0.16 | 0.52 | 0.41 | 0.13 | 0.28 | 0.15 | 0.3 | 0.24 | 0.16 |
| MnO | 0.01 | 0.005 | 0.01 | 0.02 | 0.01 | 0.005 | 0.005 | 0.01 | 0.01 | 0.01 | 0.01 | 0.005 | 0.02 | 0.01 | 0.01 |
| CaO | 0.05 | 0.03 | 0.04 | 0.04 | 0.02 | 0.02 | 0.03 | 0.04 | 0.03 | 0.03 | 0.05 | 0.02 | 0.06 | 0.04 | 0.02 |
| $Na_2O$ | 0.22 | 0.18 | 0.13 | 0.08 | 0.08 | 0.2 | 0.16 | 0.32 | 0.3 | 0.2 | 0.33 | 0.17 | 0.28 | 0.34 | 0.17 |
| $K_2O$ | 1.11 | 1.24 | 1.28 | 1.77 | 1.4 | 1.32 | 0.18 | 0.93 | 1.07 | 0.95 | 0.44 | 0.93 | 0.53 | 0.04 | 0.65 |
| $P_2O_5$ | 0.06 | 0.04 | 0.06 | 0.07 | 0.04 | 0.04 | 0.04 | 0.02 | 0.03 | 0.05 | 0.05 | 0.03 | 0.03 | 0.03 | 0.02 |
| LOI | 0.36 | 1.19 | 0.17 | 1.19 | 0.32 | 0.47 | 0.19 | 0.59 | 0.41 | 0.68 | 0.33 | 0.56 | 0.46 | 0.32 | 0.49 |
| TOTAL | 96.29 | 97.05 | 94.6 | 95.81 | 94.98 | 93.54 | 97.67 | 96.77 | 96.11 | 95.57 | 98.38 | 97.04 | 98.87 | 100.36 | 98.41 |

**Table 3**
Geochemical data showing trace elemental distribution of QPC from the study area.

| Sample/Elements (in ppm) | DP/8 | DP/81 | DP/86 | DP/90 | DP/23 | DP/2 | DP/14 | DP/28A | DP/55 | Bali/1 | Bali/8 | Bali/10 | BBL/41 | BBL/52 | BBL/70 | BBL/74 | BBL/78 | BBL/85 | BBL/90 | BBL/100 | Average |
|---|---|---|---|---|---|---|---|---|---|---|---|---|---|---|---|---|---|---|---|---|---|
| Sc | 4 | 1 | 1 | 2 | 3 | 2 | <1 | <1 | 1 | 1 | <1 | <1 | <1 | 3 | 2 | 3 | 2 | 1 | <1 | 2 | 2.07 |
| V | 100 | 39 | 31 | 69 | 28 | 59 | 59 | 9 | 11 | 15 | 17 | 28 | 33 | 71 | 38 | <5 | 22 | 15 | 11 | 52 | 37.6 |
| Cr | 580 | 298 | 239 | 535 | 173 | 436 | 349 | 134 | 125 | 119 | 142 | 200 | 180 | 360 | 190 | 195 | 125 | 121 | 94 | 369 | 251.38 |
| Co | 98 | 57 | 50 | 100 | 41 | 82 | 96 | 50 | 56 | 42 | 64 | 136 | 46 | 61 | 110 | 63 | 53 | 102 | 31 | 59 | 68.86 |
| Ni | 55 | 67 | 27 | 41 | 25 | 216 | 28 | 26 | 54 | 6 | 6 | 2 | 5 | 9 | 2 | 4 | 7 | 3 | 7 | 57 | 32.33 |
| Cu | 47 | 83 | 52 | 101 | 8 | 89 | 21 | 61 | 34 | 20 | 21 | 46 | 11 | 17 | 12 | 10 | 13 | 13 | 15 | 43 | 35.48 |
| Zn | 85 | 73 | 79 | 81 | 15 | 206 | 18 | <5 | 39 | <5 | <5 | <5 | <5 | <5 | <5 | <5 | <5 | <5 | <5 | 26 | 64 |
| Rb | 69 | 5 | 15 | <5 | 85 | 1 | 84 | 15 | 32 | 40 | 28 | 20 | 17 | 35 | 28 | 35 | 22 | 37 | 33 | 27 | 34.25 |
| Sr | 8 | <5 | 8 | 10 | 6 | <5 | 7 | 2 | <5 | <5 | 10 | <5 | <5 | <5 | <5 | 2 | 4 | 5 | 7 | 3 | 5.69 |
| Y | 158 | 94 | 51 | 118 | 45 | 111 | 97 | 26 | 37 | 26 | 9 | 6 | 58 | 106 | 56 | 62 | 51 | 24 | 21 | 89 | 62.52 |
| Zr | 278 | 98 | 77 | 193 | 135 | 178 | 205 | 41 | 58 | 52 | 47 | 59 | 102 | 186 | 100 | 126 | 62 | 56 | 23 | 182 | 116.05 |
| Nb | <5 | <5 | <5 | 3 | <5 | 15 | <5 | <5 | <5 | 6 | 6 | 14 | 5 | 3 | <5 | <5 | 32 | 7 | <5 | 7 | 9.27 |
| Ba | 101 | 5 | 103 | 5 | 175 | 5 | 132 | 31 | 14 | 55 | 42 | 15 | 14 | 5 | 22 | 52 | 53 | 75 | 81 | 24 | 49 |
| Hf | 5 | 2 | 2 | 4 | 3 | 3 | 4 | 2 | 2 | 2 | 2 | 3 | 2 | 4 | 2 | 3 | 2 | 2 | 2 | 3 | 2.76 |
| Pb | 117 | 91 | 60 | 163 | 10 | 236 | 18 | 60 | 113 | 12 | 54 | 550 | 27 | 24 | 78 | 19 | 32 | 47 | 43 | 18 | 85.1 |
| Th | 63 | 57 | 46 | 143 | 22 | 140 | 67 | 101 | 62 | 18 | 9 | 18 | 10 | 60 | 24 | 9 | 5 | 9 | 18 | 53 | 46.33 |
| U | 41 | 70 | 29 | 157 | 8 | 167 | 16 | 131 | 28 | 35 | 15 | 30 | 5 | 23 | 12 | 1 | 3 | 3 | 5 | 27 | 38.9 |

**Table 4**
Geochemical data showing trace elemental distribution of quartzites from the study area.

| Sample/ Elements (in ppm) | AK/DP/5 | AK/DP/10 | AK/DP/11 | AK/DP/16 | AK/DP/20 | AK/DP/45 | AK/DP/54 | AK/DP/64 | AK/DP/73 | AK/DP/76 | AK/DP/89 | AK/BBL/12 | AK/BBL/47 | AK/BBL/59 | AK/BBL/66 | Range | Average | UCC© | PAAS® |
|---|---|---|---|---|---|---|---|---|---|---|---|---|---|---|---|---|---|---|---|
| Sc | 2 | 2 | 2 | 4 | 2 | 3 | 1 | 2 | 3 | 3 | 1 | 2 | 2 | 1 | 2 | 1.0–3.0 | 2.13 | - | - |
| Cr | 179 | 144 | 210 | 315 | 143 | 175 | 51 | 183 | 247 | 91 | 94 | 97 | 125 | 101 | 140 | 51–315 | 153 | 80 | - |
| Ni | 11 | <5.0 | 8 | 18 | 10 | <5.0 | 13 | 14 | 8 | <5.0 | <5.0 | <5.0 | 5 | 6 | 8 | <5.0–18 | 10.1 | 20 | 55 |
| Cu | 14 | 6 | 7 | 12 | 13 | 7 | 9 | 12 | 10 | 10 | 10 | 7 | 9 | 5 | 10 | 5.0–14 | 9.4 | 25 | 50 |
| Rb | 74 | 11 | 38 | 97 | 69 | 80 | 39 | 53 | 42 | 45 | 48 | 50 | 37 | 28 | 31 | 11–97 | 49.47 | 112 | 160 |
| Y | 14 | 11 | 15 | 28 | 14 | 6 | 4 | 4 | 5 | 3 | 3 | 4 | 6 | 6 | 6 | 3.0–28 | 8.6 | 22 | 27 |
| Zr | 139 | 115 | 195 | 212 | 89 | 161 | 67 | 104 | 139 | 74 | 92 | 96 | 97 | 108 | 68 | 67–212 | 117.07 | 190 | 210 |
| Ba | 336 | 343 | 275 | 319 | 195 | 171 | 82 | 131 | 172 | 113 | 193 | 126 | 115 | 114 | 120 | 82–343 | 187 | 550 | 650 |
| Hf | 3 | 4 | 7 | 5 | 3 | 3 | 2 | 3 | 3 | 2 | 2 | 3 | 3 | 3 | 2 | 2.0–7.0 | 3.2 | 5.8 | 5 |
| Pb | 26 | 79 | 52 | 20 | 12 | 5 | 5 | 5 | 5 | 5 | 5 | 5 | 5 | 5 | 5 | 5.0–79 | 15.93 | 20 | 20 |
| Th | 26 | 13 | 17 | 25 | 7 | 6 | 1 | 4 | 5 | 2 | 1 | 3 | 5 | 4 | 7 | 1.0–26 | 8.33 | 10.7 | 14.6 |
| U | 12 | 5 | 6 | 7 | 3 | 2 | 1 | 2 | 2 | 1 | 1 | 2 | 2 | 1 | 4 | 1.0–12 | 3.4 | 2.8 | 3.1 |

**Table 5**
REE distribution within QPC from the study area.

| Sample/ Elements (in ppm) | DP/8 | DP/81 | DP/86 | DP/90 | DP/23 | DP/2 | DP/14 | DP/28A | DP/35 | DP/55 | Bali/1 | Bali/8 | Bali/10 | BBL/41 | BBL/52 | BBL/70 | BBL/74 | BBL/78 | BBL/85 | BBL/90 | BBL/100 | Range | Average | UCC© | PAAS® |
|---|---|---|---|---|---|---|---|---|---|---|---|---|---|---|---|---|---|---|---|---|---|---|---|---|---|
| La | 198 | 200 | 94 | 325 | 51 | 230 | 110 | 43 | 83 | 45 | 16 | 32 | 51 | 62 | 107 | 76 | 46 | 31 | 38 | 27 | 82 | 16–325 | 92.7 | 30 | 38 |
| Ce | 293 | 317 | 158 | 534 | 68 | 406 | 169 | 69 | 133 | 69 | 29 | 39 | 81 | 103 | 186 | 123 | 80 | 47 | 54 | 44 | 142 | 29–534 | 149.7 | 64 | 80 |
| Pr | 23 | 20 | 12 | 32 | 7 | 24 | 12 | 5 | 10 | 5 | 2 | 4 | 8 | 8 | 16 | 10 | 4 | 1 | 1 | 2 | 10 | 1.0–32 | 10.3 | 7.1 | 8.9 |
| Nd | 135 | 130 | 68 | 224 | 32 | 162 | 74 | 30 | 57 | 27 | 7 | 15 | 39 | 44 | 82 | 51 | 33 | 21 | 21 | 18 | 62 | 7.0–224 | 63.4 | 26 | 32 |
| Sm | 31 | 29 | 15 | 48 | 7 | 36 | 16 | 6 | 12 | 5 | 2 | 3 | 10 | 9 | 20 | 10 | 8 | 5 | 7 | 6 | 14 | 2.0–48 | 14.2 | 4.5 | 5.6 |
| Eu | 1.1 | 1 | 0.6 | 0.8 | 0.5 | 0.9 | 0.5 | 0.5 | <0.5 | <0.5 | <0.5 | <0.5 | 0.6 | <0.5 | 0.9 | <0.5 | <0.5 | <0.5 | <0.5 | <0.5 | <0.5 | <0.5–1.1 | 0.74 | 0.88 | 1.1 |
| Gd | 2.8 | 25 | 12 | 37 | 7 | 30 | 17 | 5 | 11 | 4 | 2 | 3 | 8 | 7 | 19 | 11 | 8 | 6 | 5 | 6 | 14 | 2.0–37 | 11.4 | 3.8 | 4.7 |
| Tb | 1.8 | 1.4 | 0.8 | 1.7 | 0.8 | 1.4 | 1 | <0.5 | 0.7 | <0.5 | <0.5 | <0.5 | 0.5 | 0.5 | 0.7 | 0.5 | <0.5 | <0.5 | <0.5 | <0.5 | 0.5 | <0.5–1.8 | 0.95 | 0.64 | 0.77 |
| Dy | 20 | 14 | 7 | 20 | 5 | 18 | 10 | 3 | 7 | 2 | 2 | 2 | 3 | 3 | 12 | 8 | 6 | 2 | 2 | 2 | 10 | 2.0–20 | 7.5 | 3.5 | 4.4 |
| Ho | 3 | 3 | 1 | 3 | 2 | 3 | 2 | 0.5 | 0.6 | <0.5 | 0.6 | 2 | 0.6 | 0.5 | 2 | 1 | <0.5 | 1 | 1 | 1 | 1 | <0.5–3.0 | 1.5 | 0.8 | 1 |
| Er | 13 | 7 | 3 | 11 | 3 | 10 | 8 | 1 | 5 | 1 | 1 | 1 | 2 | 1 | 10 | 5 | 2 | 1 | 1 | 1 | 7 | 1.0–13 | 4.5 | 2.3 | 2.9 |
| Tm | 1.1 | 0.8 | 0.7 | 0.6 | 0.6 | 0.5 | 0.5 | <0.5 | <0.5 | <0.5 | <0.5 | <0.5 | <0.5 | <0.5 | 0.5 | <0.5 | <0.5 | <0.5 | <0.5 | <0.5 | <0.5 | <0.5–1.1 | 0.66 | 0.33 | 0.4 |
| Yb | 11 | 5 | 2 | 8 | 3 | 7 | 5 | 2 | 4 | <0.5 | <0.5 | <0.5 | 0.6 | 2 | 8 | 5 | 4 | 3 | <0.5 | 2 | 0.6 | <0.5–11 | 4.3 | 2.2 | 2.8 |
| Lu | 1.3 | 1.1 | 0.6 | 0.8 | 0.7 | 0.9 | 0.6 | <0.5 | <0.5 | <0.5 | <0.5 | <0.5 | 0.6 | 0.5 | 1 | 0.5 | 0.5 | 0.5 | <0.5 | <0.5 | 0.6 | <0.5–1.3 | 0.73 | 0.32 | 0.43 |
| ΣREE | 760 | 754.3 | 374.7 | 1246 | 185.6 | 830 | 425.6 | 165 | 323.3 | 158 | 61.6 | 101 | 205.4 | 240.5 | 464.1 | 301 | 189.5 | 118.5 | 130 | 109 | 343.1 | 61.6–1246 | 356.5 | 146.37 | 183 |
| Y | 103 | 82 | 25 | 90 | 28 | 91 | 58 | 18 | 44 | 5 | 8 | 9 | 10 | 23 | 76 | 46 | 39 | 31 | 14 | 18 | 54 | 5.0–130 | 41.5 | 22 | 27 |
| LREE | 680 | 696 | 347 | 1163 | 165 | 858 | 381 | 153 | 295 | 151 | 56 | 93 | 189 | 226 | 411 | 270 | 171 | 105 | 121 | 97 | 310 | 56–1193 | 330.4 | 131.6 | 164.5 |
| HREE | 39.7 | 56.2 | 26.5 | 81.3 | 26.4 | 69.9 | 43.5 | 11.5 | 28.3 | 7 | 5.6 | 8 | 14.7 | 14 | 52.2 | 30.5 | 20 | 13 | 9 | 12 | 33.1 | 9.0–81.3 | 28.68 | 13.57 | 16.97 |
| LREE/HREE | 17.1 | 12.38 | 13.09 | 14.31 | 6.25 | 12.3 | 8.76 | 13.3 | 10.42 | 21.57 | 10 | 11.6 | 12.86 | 16.14 | 7.87 | 8.85 | 8.55 | 8.08 | 13.44 | 8.08 | 9.36 | 7.87–21.57 | 11.16 | 9.7 | 9.69 |

**UCC**©: Average of Upper Continental Crust; **PAAS**®: Average of Post Archean Australian Shale (Values after Taylor and McLennan, 1985).

**Table 6**
REE distribution within quartzites from the study area.

| Sample/Elements (in ppm) | DP/5 | DP/10 | DP/11 | DP/16 | DP/20 | DP/45 | DP/54 | BBL/12 | BBL/47 | BBL/59 | BBL/66 | DP/64 | DP/73 | DP/76 | DP/89 | Range | Average | UCC© | PAAS® |
|---|---|---|---|---|---|---|---|---|---|---|---|---|---|---|---|---|---|---|---|
| La | 45 | 27 | 29 | 52 | 20 | 18 | 5 | 13 | 15 | 9 | 25 | 18 | 22 | 12 | 12 | 5.0–52 | 21.8 | 30 | 38 |
| Ce | 100 | 50 | 57 | 109 | 40 | 44 | 13 | 31 | 27 | 19 | 45 | 32 | 41 | 20 | 19 | 13–109 | 43.13 | 64 | 80 |
| Pr | 3 | <1 | <1 | 10 | 5 | 5 | 1 | 4 | 3 | 2 | 5 | 4 | 5 | 2 | 2 | <1.0–10 | 3.4 | 7.1 | 8.9 |
| Nd | 34 | 19 | 23 | 37 | 18 | 18 | 6 | 12 | 11 | 7 | 15 | 13 | 15 | 7 | 8 | 6.0–37 | 16.2 | 26 | 32 |
| Sm | 7 | 4 | 5 | 8 | 5 | 5 | 1 | 2 | 2 | 1 | 4 | 2 | 3 | 1 | 2 | 1.0–8.0 | 3.46 | 4.5 | 5.6 |
| Eu | <0.5 | <0.5 | <0.5 | 0.8 | 0.6 | 0.7 | <0.5 | <0.5 | <0.5 | <0.5 | 0.7 | <0.5 | 0.5 | <0.5 | <0.5 | <0.5–0.8 | – | 0.88 | 1.1 |
| Gd | 7 | 4 | 5 | 7 | 4 | 4 | 1 | 2 | 2 | 2 | 4 | 2 | 3 | 1 | 1 | 1.0–7.0 | 3.26 | 3.8 | 4.7 |
| Tb | <0.5 | <0.5 | <0.5 | 0.9 | 0.7 | 0.5 | <0.5 | <0.5 | <0.5 | <0.5 | 0.5 | <0.5 | <0.5 | <0.5 | <0.5 | <0.5–0.9 | – | 0.64 | 0.77 |
| Dy | 4 | 3 | 4 | 5 | 3 | 3 | 1 | 2 | 1 | 2 | 3 | 2 | 2 | 1 | 1 | 1.0–5.0 | 2.46 | 3.5 | 4.4 |
| Ho | 0.7 | 0.6 | 0.8 | 0.9 | 0.5 | <0.5 | <0.5 | <0.5 | <0.5 | <0.5 | 0.5 | <0.5 | <0.5 | <0.5 | <0.5 | <0.5–0.9 | – | 0.8 | 1 |
| Er | 2 | 2 | 2 | 2.5 | 0.9 | 0.5 | <0.5 | <0.5 | <0.5 | <0.5 | 1.3 | <0.5 | 0.8 | <0.5 | <0.5 | <0.5–2.5 | – | 2.3 | 2.9 |
| Tm | <0.5 | <0.5 | 0.5 | <0.5 | <0.5 | <0.5 | <0.5 | <0.5 | <0.5 | <0.5 | <0.5 | <0.5 | <0.5 | <0.5 | <0.5 | <0.5–0.5 | – | 0.33 | 0.4 |
| Yb | 3.2 | 2.3 | 3.3 | 2.4 | 0.5 | <0.5 | <0.5 | 0.5 | 0.5 | <0.5 | 0.8 | <0.5 | <0.5 | <0.5 | <0.5 | <0.5–3.3 | – | 2.2 | 2.8 |
| Lu | 0.6 | 0.5 | 0.7 | 0.4 | <0.5 | <0.5 | <0.5 | <0.5 | <0.5 | <0.5 | <0.5 | <0.5 | <0.5 | <0.5 | <0.5 | <0.5–0.7 | – | 0.32 | 0.43 |
| ∑REE | 206.5 | 112.4 | 130.3 | 235.9 | 98.2 | 98.7 | 28 | 66.5 | 61.5 | 42 | 104.8 | 73 | 92.3 | 44 | 45 | 28–235.9 | 95.94 | 146.37 | 183 |
| Y | 14 | 11 | 15 | 28 | 14 | 6 | 4 | 4 | 6 | 6 | 6 | 4 | 5 | 3 | 3 | 3.0–28 | 8.6 | 22 | 27 |

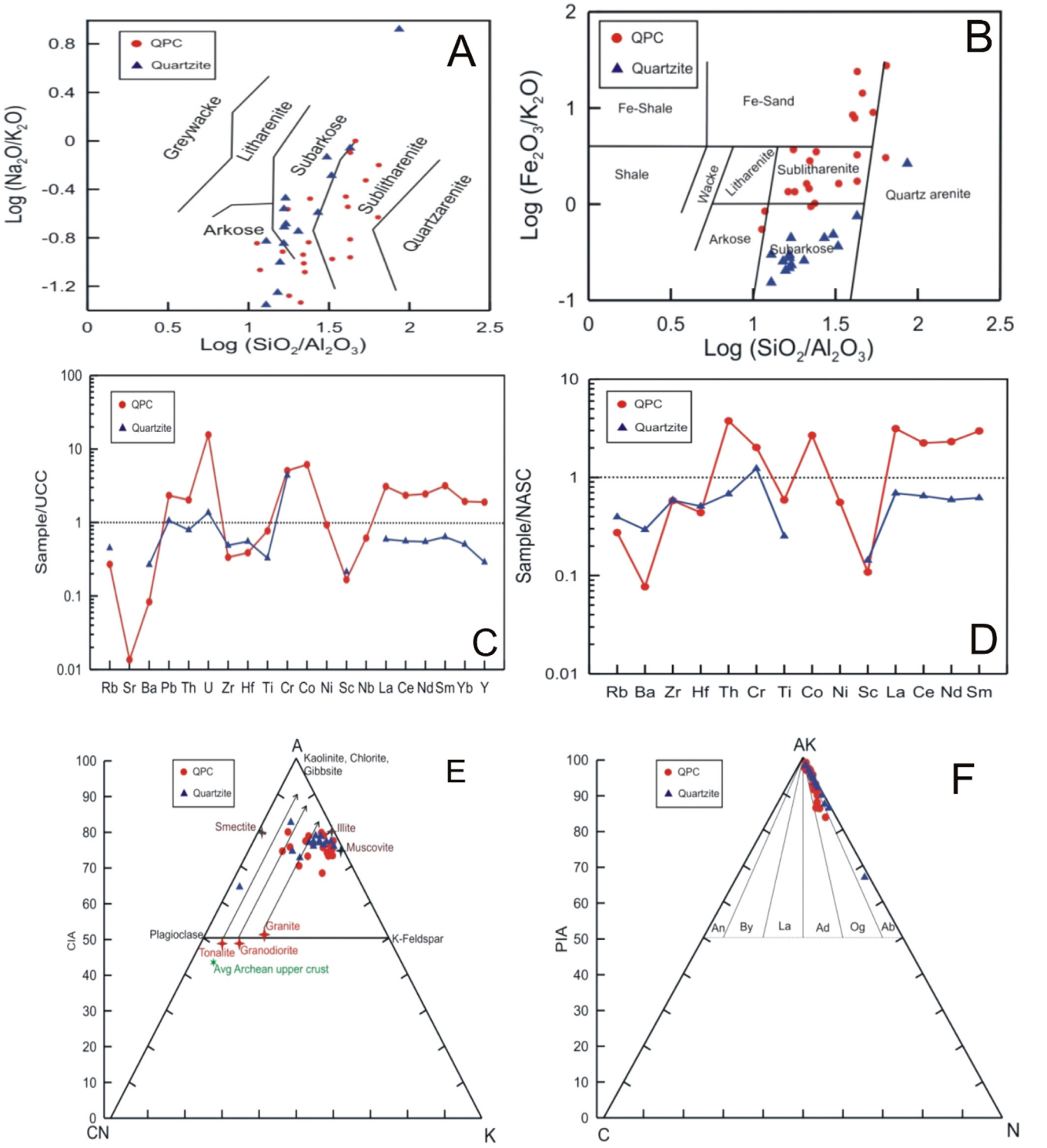


**Fig. 3.** Geochemical variation diagrams of QPC and quartzites indicating the source characterization and their possible provenance; A) Chemical classification of QPC and quartzites on Log ($SiO_2/Al_2O_3$) vs Log ($Na_2O/K_2O$) diagram (fields after Pettijohn et al., 1972); B) Chemical classification of the QPC and quartzites based on Log ($SiO_2/Al_2O_3$) vs Log ($Fe_2O_3/K_2O$) (fields after Heron, 1988). Note that most of the samples of QPC predominantly fall within the Sublitharenite field while the quartzites are within the Subarkosic field; C) Trace element distribution patterns in QPC and quartzites, western margin of Bonai Granite, Orissa with respect to UCC; D) Trace element distribution patterns in QPC and quartzites, western margin of Bonai Granite, Orissa with respect to NASC; E) A-CN-K ($Al_2O_3$–$CaO^*$ + $Na_2O$–$K_2O$) ternary diagram, after Nesbitt and Young (1982) and the arrow shows the trend of weathering and alteration ($CaO^*$-CaO in silicates only). Data on granite, granodiorite, tonalite and Archean upper crust are from Condie (1993); F) QPC and quartzites samples fall within the fields of alkali feldspar in the AK-C-N ternary diagram (Fedo et al., 1995).

from 0.09 to 0.31(mean = 0.23) and 0.04 to 0.27 (mean = 0.21) for quartzites. The potassic nature of QPC and quartzite is reflected by high $K_2O/Na_2O$ ratios which ranges from 1.25 to 19.0 (mean = 5.94) and 0.12 to 22.12 (mean = 4.38) respectively (Tables 1 and 2). $K_2O/Al_2O_3$ ratio of terrigenous sedimentary rocks was used to decipher the original composition of ancient sediments, because the ratio for clay minerals and feldspars are different (Cox et al., 1995). The $K_2O/Al_2O_3$ ratio for clay minerals is up to

0.3 and for feldspar, it ranges from 0.3 to 0.9. In both QPC and quartzites, low values of $K_2O/Al_2O_3$ ratio indicate the presence of clay minerals and not feldspar which is corroborated by their petrographic characteristics.

### 5.1. Trace elemental variations

The signature of trace elements is mainly dependent on the minerals where these elements reside. It has been shown by many workers that most of the trace elements in clastic rocks reside in clay minerals (Taylor and McLennan, 1985; Condie, 1993). The role of accessory minerals in the trace element geochemistry has also been discussed and recognized by many researchers (Yan et al., 2000; Singh and Rajamani, 2001). Trace element data of QPC and quartzites are given in Tables 3 and 4. Among trace elements, U in QPC ranges from 1.0 to 167 ppm while Th shows variation from 5.0 to 143 ppm which is higher than the U, Th contents in both Upper Continental Crust (UCC) and Post-Archean Australian Shale (PAAS) (Table 4). In quartzites, U and Th values vary from 1.0 to 12 ppm and Th from 1.0 to 26 ppm (Table 4). Thus, both QPC and quartzites in the study area are enriched in U and Th with respect to UCC and PAAS, however, U and Th enrichment is more in QPC than in quartzites. High U and Th contents in QPC can be explained due to the presence of detrital uraninite and monazite grains in their matrix and presence of secondary uranyl minerals and adsorbed uranium associated with goethite, limonite, hematite and anatase (Kumar et al., 2012).

Concentration of Rb, Ba and Sr are low in QPC and quartzites with respect to UCC and PAAS reflecting scarcity of K-feldspar and Ca-rich feldspar. Low Rb/Sr indicates alteration and weathering of feldspar either in the source area or during transportation of sediments. Cr content in both QPC (94–580 ppm) and quartzites (51–315 ppm) is higher than UCC and PAAS (Tables 3 and 4). The high concentration of Cr is due to presence of chromite and fuchsite mica in matrix of QPC and only fuchsite in quartzite which is supported by the presence of chromite during SEM- EDS studies (Kumar, 2013).

## 6. U, Th, Au and Pt in QPC and quartzites

QPC and quartzites samples have been analyzed using ICP-MS for uranium and thorium. Radioactive QPC indicate U from 1.0–167 ppm, Th from 5–143 ppm, whereas in quartzites U varies from 1.0 to 19 ppm and Th varies from 1.0 to 35 ppm. Au values in QPC show variation from < 20 ppb to 382 ppb. Out of twenty-one samples, eight samples indicated < 20 ppb of Au whereas rest thirteen samples revealed elevated concentration of Au ranging from 30 to 382 ppb which is on higher side compared to crustal abundance of 4 ppb. Some of the higher values of Au in QPC are 142, 246, 261 and 382 ppb. Fourteen samples of quartzites indicate higher concentration of Au varying from 30 ppb to 1527 ppb, with some of them are showing relatively higher values like 233, 238, 264, 557 and 1527 ppb. PGE contents were analyzed on selected five samples of QPC and quartzites containing higher concentration of gold. Out of five, three samples of QPC indicate <10 ppb of Pt, two samples indicate 15 to 188 ppb of Pt. Similarly out of five, two samples in quartzites analyzed <10 ppb Pt and the rest three samples have shown 220, 245 and 692 ppb of Pt which is significant (Kumar et al., 2011).

La and Ce when compared to UCC indicates towards mixed source (Cingolani et al., 2003). The presence of detrital chromite grains and higher concentration of Cr indicate their derivation partly from mafic–ultramafic source rocks. Gorumahisani-Badampahar and Daitari-Tomka which is considered to have such older mafic–ultramafic sequences (Mukhopadhyay et al., 2008, 2014) could be the source for Cr and minor Ni and Co in QPC (Haque et al., 2001).This indicates that QPC-quartzites in the area is certainly younger than IOG rocks which is supplying Cr, Ni and Co to them.

QPC generally show enrichment of Pb, Th, U, Cr, Co, Ni, La, Ce, Nd, Sm, Yb and Y with respect to Upper Continental Crust (UCC) whereas quartzite show slight enrichment only in Pb, U and Cr. In contrast to REE enrichment in QPC, quartzites show depletion in REE with respect to both UCC and North American Shale Composite (NASC) and both show depletion in Rb, Sr, Ba and Sc with respect to UCC and NASC. QPC also indicate enrichment of Th, Cr, Co and REE with depletion in Rb, Ba, Ti, Ni, Sc with respect to NASC (Fig. 3C and D).

REE distribution in QPC and quartzites are given in Tables 5 and 6. Total REE in QPC ranges from 62 to 1246 ppm, whereas in quartzites, REE ranges from 28 to 236 ppm, thus point towards enrichment of REE in QPC than in quartzites. Total REE content in QPC show enrichment compared to UCC and PAAS. On the other hand, quartzites show depletion in total REE with respect to UCC and PAAS. Yttrium (Y) in QPC range from 5.0 to 130 ppm which is 1.5 to 2.0 times more than UCC and PAAS. Y vary from 3.0 to 28 ppm with a mean of 8.6 in quartzites which is about 3 times lower than the values in UCC and PAAS. High LREE/HREE ratio is observed in felsic rocks whereas low LREE/HREE ratios have been noted in mafic rocks (Cullers and Graf, 1983). In the present study, higher LREE/HREE ratios exhibited by QPC over the UCC and PASS indicate felsic provenance (Table 5).

## 7. Paleo-weathering history of QPC- quartzite sequence

Paleo-weathering history can be reconstructed based on various geochemical parameters. We have addressed this aspect for QPC-quartzite sequence from western part of SOC, while Ghosh et al. (2016), reconstructed the paleo-weathering and provenance from eastern part of SOC. The degree of chemical weathering and nature of source rock for sediments can be assessed by knowing chemical index of alteration (CIA) (Nesbitt and Young, 1982, 1984). Similarly effects of chemical weathering can also be envisaged using A-CN-K diagram which provides information on the change in the bulk composition of the probable source rock of sediments during weathering. Alterations of minerals in the sediments represent the intensity and duration of chemical weathering processes which were operative in the source area. The weathering history of the provenance or source-rock has been deduced from the quantitative measurement of chemical weathering of silicates by calculating Chemical Index of Alteration (CIA) and Plagioclase Index of Alteration (PIA) (Nesbitt and Young, 1982, 1984; Fedo et al., 1995; Akarish and EL-Gohary, 2011). Chemical Index of Alteration: (CIA) represents a ratio of predominantly immobile $Al_2O_3$ to the mobile cations $Na^+$, $K^+$ and $Ca^{2+}$ given as oxides. The CIA is defined as: $*\mathbf{CIA} = 100(Al_2O_3)/(Al_2O_3 + CaO + Na_2O + K_2O)$; where the amount of CaO is that portion which is incorporated in the silicate fraction of the rock. The resultant CIA gives a measure of the proportion of secondary aluminous clay minerals to primary silicate minerals such as feldspars (Nesbitt and Young 1982).

The Chemical Index of Alteration (CIA) values actually reflect the intensity of chemical weathering in the source region (Nesbitt and Young 1982). Fedo et al. (1995) mentioned that the CIA value of 50–60 indicates an incipient weathering, CIA 60–80 intermediate weathering and CIA > 80 extreme weathering. Several workers have used CIA to decipher degree of weathering in Precambrian pelitic rocks (Wronkiewicz and Condie, 1989; Ghosh et al. 2016). Degree of weathering is a function chiefly of climate and rate of tectonic uplift (Wronkiewicz and Condie, 1987). Increased chemical weathering may reflect the decrease in tectonic

**Table 7**
Chemical Index of Alteration (CIA) and Plagioclase Index of Alteration (PIA) of radioactive QPC and Quartzites from the study area.

| Lithounits | QPC | | Quartzites | | |
|---|---|---|---|---|---|
| Sample No | CIA = A/(ACNK) * 100 | PIA = A-K/(CAN-K) * 100 | Sample No | CIA = A/(ACNK) * 100 | PIA = A-K/(CAN-K) * 100 |
| DP/8 | 74.75 | 94.74 | AK/DP/5 | 76.81 | 91.41 |
| DP/81 | 75.27 | 82.15 | AK/DP/10 | 76.18 | 92.8 |
| DP/86 | 78.34 | 89.54 | AK/DP/11 | 77.14 | 94.62 |
| DP/90 | 79.46 | 85.12 | AK/DP/16 | 75.77 | 96.48 |
| DP/23 | 73.7 | 91.54 | AK/DP/20 | 77.2 | 96.5 |
| DP/2 | 74.15 | 79.6 | AK/DP/45 | 78.64 | 93.77 |
| DP/14 | 75.79 | 94.85 | AK/DP/54 | 82.47 | 88.04 |
| DP/28A | 75.15 | 91.42 | AK/DP/64 | 76.86 | 88.4 |
| DP/35 | 78.48 | 94.73 | AK/DP/73 | 75.84 | 88.88 |
| DP/55 | 76.95 | 87.5 | AK/DP/76 | 78.79 | 92.17 |
| Bali/1 | 75.99 | 88.89 | AK/DP/89 | 74.47 | 81.98 |
| Bali/8 | 72.73 | 84.18 | AK/BBL/12 | 77.22 | 92.15 |
| Bali/10 | 70.07 | 79.29 | AK/BBL/47 | 72.66 | 82.07 |
| BBL/41 | 68.04 | 83.39 | AK/BBL/59 | 64.54 | 65.29 |
| BBL/52 | 76.96 | 97.35 | AK/BBL/66 | 77.22 | 90.05 |
| BBL/70 | 72.9 | 92.97 | – | – | – |
| BBL/74 | 72.8 | 91.14 | – | – | – |
| BBL/78 | 73.19 | 92.15 | – | – | – |
| BBL/85 | 75.33 | 94.64 | – | – | – |
| BBL/90 | 73.95 | 92.62 | – | – | – |
| BBL/100 | 75.33 | 94.55 | – | – | – |
| Average | 74.73 | 89.64 | Average | 76.12 | 88.97 |

activity and/or the change of climate towards warm and humid conditions favouring enhanced chemical weathering in the source region (Jacobson et al., 2003). Therefore, weathering indices of sedimentary rocks can provide useful information about the source area tectonic activity and climatic conditions.

Maynard et al. (1991) applied CIA to infer weathering in sand-sized clastic rocks, mainly on Witwatersrand quartzites. It has also been observed by Maynard et al. (1991) that in Witwatersrand basin which host QPC type Au-U deposit, where grade of both uranium and gold increases with increasing quartz and therefore, the process responsible for enrichment of quartz in the sediments were responsible for uranium stability. Thus, paleo-weathering study will be helpful in deciphering the conditions of deposition of sediments and in turn, preservation of detrital uraninite and pyrite in them.

The CIA values on 21 samples of QPC and 15 quartzites were calculated based on the given formula. The CIA values for QPC and quartzites are given in Table 7. CIA values for QPC range from 68.04 to 79.46 and for quartzites, this value show variation from 64.54 to 82.47. Based on CIA values it can be inferred that QPC and quartzites of the study area has undergone moderate to high degree of chemical weathering. Archean sediments generally display low CIA values indicating a relatively un-weathered source and an active tectonic uplift. Our study has indicated moderate to high CIA which is comparable to reported values from Mesoarchean siliciclastic successions from Keonjhar area of SOC (Ghosh et al., 2016). These values inferred to be of cratonic affinity as shown from Pongola Supergroup (CIA 71–86) and Witwatersrand Supergroup (CIA average of 83) (Wronkiewicz and Condie, 1989).

In the A-CN-K diagram, majority of the QPC and quartzite samples cluster along the A-K line nearby illite-muscovite (Fig. 3D) field which also indicate weathering trend of granite, granodiorite and tonalite are shown at the base of plagioclase-K-feldspar line. These trend line and points on A-CN-K diagram when traced back, provide information about the source of the sedimentary suites. The majority of samples indicate granite source, a few samples between granite and granodiorite-tonalite and rarely near tonalite and plagioclase-kaolinite fields (Fig. 3E). The geology of Singhbhum-Orissa Craton expose different types of granitic rocks ranging from granite to tonalite south of the study area (Saha, 1994) which might have provided the detritus to these sediments during the upliftment, erosion and moderate rates of chemical weathering.

### 7.1. Plagioclase Index of alteration (PIA)

The degree of chemical weathering can also be estimated by using PIA (Fedo et al., 1995) in molecular proportions and the PIA can be worked out as: : **PIA** = $(Al_2O_3\text{-}K_2O)/(Al_2O_3 + CaO^* + Na_2O\text{-}K_2O) \times 100$, where $CaO^*$ is CaO only reside in silicate fractions. It is evident that the PIA for QPC ranges from 79.29 to 97.35 while for quartzites, the PIA range varies from 65.29 to 96.50, thus revealing high degree of plagioclase alteration and their complete dissolution (Table 7). In AK-C-N ternary diagram, all samples of QPC and quartzites range between oligoclase (Og) and albite (Ab) area (Fig. 3F). This indicates that in most of samples, plagioclase has been near complete alteration. Thus in the study area, CIA and PIA show moderate degree of chemical alteration and high plagioclase index of alteration for QPC and quartzites deposited around western margin of Bonai Granite.

### 7.2. Provenance study for QPC and quartzites

Geochemistry provides important information in provenance determination especially for the fine grained sedimentary rocks (McLennan et al. 1993). Taylor and Mclennan (1985) suggested that composition of source rock is the most dominant factor which controls the mineralogical composition of sediments derived from them, however, secondary processes like weathering, transport and diagenesis may affect chemical composition of the sediments (Wronkiewicz and Condie, 1987). La, Ce, Nd, Y, Th, Zr, Hf, Nb, Ti and Sc are most suited elements for provenance and tectonic setting determinations because of their relatively lower mobility during sedimentary processes/subsequent alteration and their low residence time in sea water (Holland, 1984).

$TiO_2$ vs Ni (Fig. 4A) indicate felsic provenance for the QPC and quartzites (Floyd et al. 1989). La-Th-Sc (Condie, 1993), all samples of QPC and quartzites plot along the La-Th line, mostly towards La (Fig. 4B). In Th/Sc vs Sc plot, both QPC and quartzites occupy the field close to granite and sandstone and away from the field of

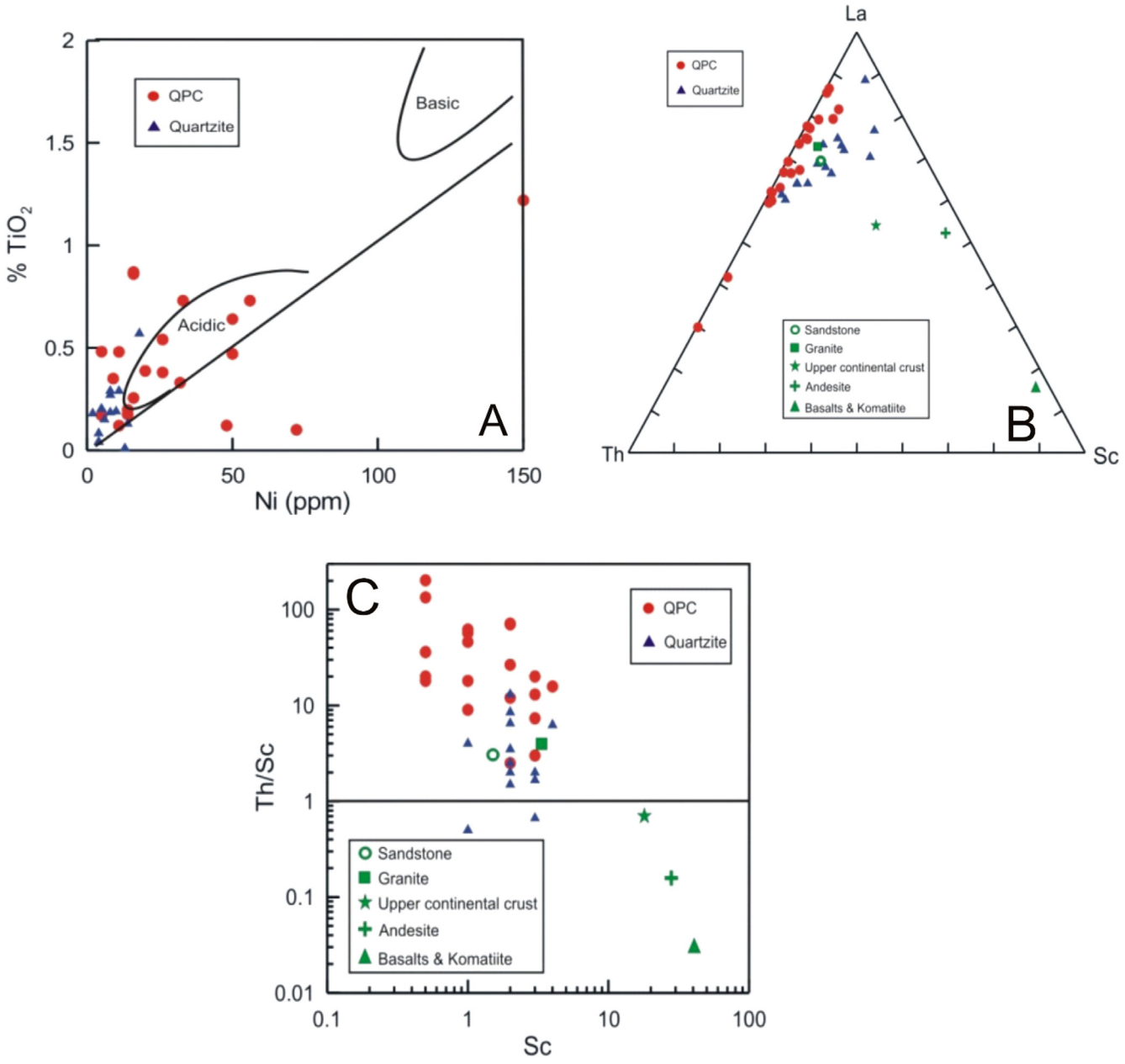


**Fig. 4.** Geochemical signatures of important trace elements depicting a strong felsic source/provenance for radioactive QPC and quartzites as seen from: A) $TiO_2$ vs Ni sedimentary provenance diagram of QPC and quartzites. (After Floyd et al., 1989); B) La-Th-Sc ternary diagram of QPC and quartzites; C) Th/Sc vs Sc binary plot of QPC and quartzites falling within the sandstone and granite fields (Values of UCC from McLennan, 2001 and sandstone, andesite, basalt and komatiite fields are from Condie, 1993).

basalt, andesite and komatiite, thus revealing felsic source for QPC and quartzites (Fig. 4C).

### 7.3. REE in provenance study

REE concentration in clastic sediments reflects the provenance and has been used to infer source rock characterization because of their relatively low mobility during weathering, transport, diagenesis, and metamorphism (Holland, 1984). They are transported chiefly as particulate matter and reflect the chemistry of their source rocks. The REE patterns have also been used to infer sources of sedimentary rocks, since basic rocks contain low LREE/HREE ratios, whereas more silicic rocks usually contain higher LREE/HREE ratios and negative Eu anomalies (Cullers and Graf, 1983). Therefore, the REE patterns of the source rocks may be preserved in sedimentary rocks (Taylor and McLennan, 1985; Wronkiewicz and Condie, 1987, 1989). The Eu anomaly in sedimentary rocks is usually interpreted as being inherited from igneous source rocks (McLennan and Taylor, 1991; Taylor and McLennan, 1985).

The REE plots for QPC and quartzites are shown in Fig. 5A to D respectively. QPC exhibit enrichment of LREE with almost flat HREE, while REE are relatively fractionated in quartzites with depleted HREE. LREE enrichment is due to the presence of monazite grains in QPC as observed from petrographic study and further corroborated by mineral chemistry (Kumar, 2013). LREE enrichment in QPC and quartzites are also reflected by their high values of $(La/Sm)_{CN}$ values ranging from 3.18–4.55 in QPC and 1.87–9.12 in quartzites and nearly flat HREE pattern with $(Gd/Yb)_{CN}$ ranging from 1.08–4.85 in QPC. Both QPC and quartzites show fractionated REE pattern, $(La/Yb)_n$ 5.77–31.93 in QPC and

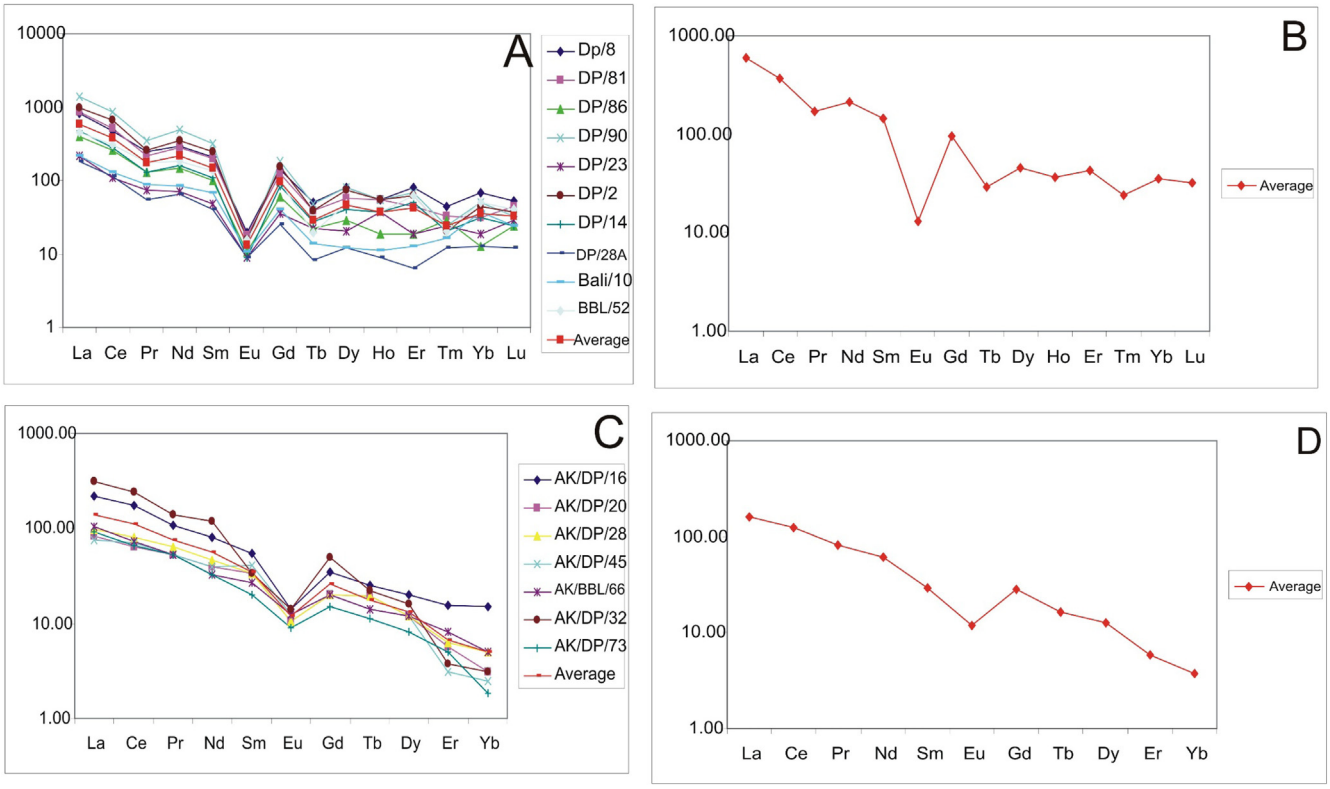


**Fig. 5.** Chondrite normalized REE patterns of QPC and quarzites showing: A) Fractionated LREE, strong negative Eu anomaly with flat HREE patterns of QPC from the study area; B) Corresponding average REE plot of QPC; C) Highly fractionated REE pattern showing enriched LREE and depleted HREE with a strong Eu anomaly of quartzites from western margin of Bonai Granite (Chondrite values are after McDonough and Sun, 1995); D) Corresponding average REE pattern of quartzites showing negative Eu anomaly (Chondrite values are after McDonough and Sun, 1995).

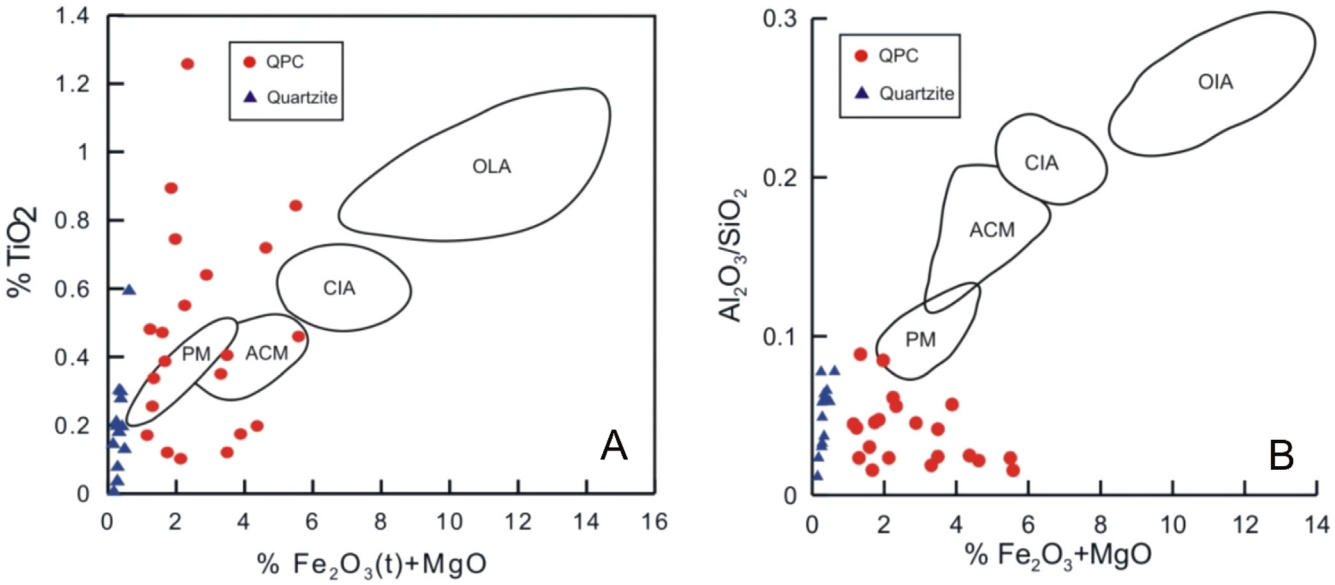


**Fig. 6.** QPC and quartzite samples fall close to the passive margin tectonic setting as seen from; A) $Fe_2O_3$ (T) +MgO vs $TiO_2$ plot; B) $Fe_2O_3$ + MgO vs $Al_2O_3/SiO_2$ (after Bhatia, 1983);

14.71–99.18 for quartzites. Moderate to strong negative Eu anomaly (0.06–0.28) in QPC and moderate negative Eu anomaly (0.33–0.54) in quartzites supports the above inference.

The presence of negative Eu anomaly has been attributed to the presence of Eu- depleted felsic igneous rocks in the provenance such as granites. QPC is generally characterized by significant depletion of Eu in chondrite- normalised REE pattern, higher concentration of total REE and increase in Th/Sc (Bhushan and Sahoo, 2010). High Th, U, La values together with fractionated chondrite normalized REE pattern and negative Eu anomaly suggest granitic provenance for QPC-quartzite sequence in the study area.

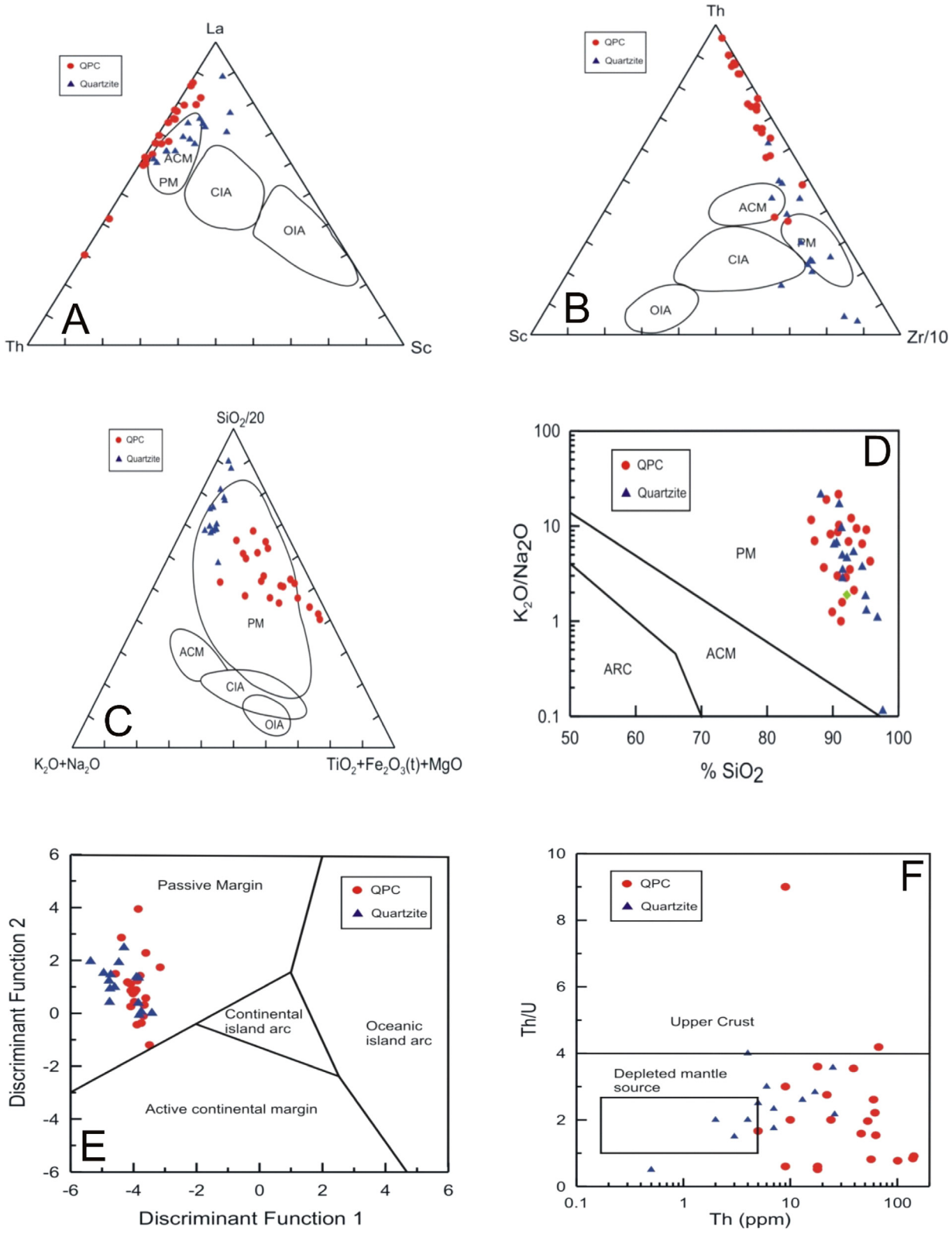


**Fig. 7.** Geochemical diagrams of radioactive QPC and quartzite samples showing passive margin tectonic affinity and enriched uranium values as noted from; A) La-Th-Sc diagram for QPC matrix and quartzites (Bhatia and Crook, 1986). B) Th-Sc-Zr ternary plot showing passive margin tectonic setting for QPC and quartzites (Bhatia and Crook, 1986); C) Plot of QPC and quartzites on $SiO_2$-$K_2O$ + $Na_2O$-$TiO_2$ + $Fe_2O_3$ (t) + MgO ternary diagram (Kroonberg, 1994); D) $K_2O/Na_2O$ vs $SiO_2$ plot of QPC and quartzites depicting predominant passive margin setting (Roser and Korsch, 1986). Data for average Proterozoic sandstone (Closed green circle) are from Condie (1993); E) Possible tectonic setting for QPC and quartzites based on discriminant function, DF-1 vs DF-2 plot (Bhatia, 1983); F) QPC and quartzites representing low Th/U ratios suggesting the enrichment of uranium as seen from the Th/U versus Th diagram (McLennan et al., 1993). Index: OIA – oceanic island arc, CIA – continental island arc, PM and ACM–passive margin/Active continental margin. DF-1 = (−0.0447 × $SiO_2$%) + (−0.972 × $TiO_{2\%}$) + (0.008 × $Al_2O_{3\%}$) + (−0.267 × $Fe_2O_3$%) + (0.208 × FeO%) + (−3082 × MnO%) + (0.104 × MgO%) + (0.195 × CaO%) + (0.719 × $Na_2O$%) + (−0.032 × $K_2O$%) + (7.510 × $P_2O_5$%). DF-2 = (−0.421 × $SiO_2$%) + (1.998 × $TiO_{2\%}$) + (−0.526 × $Al_2O_{3\%}$) + (−0.551 × $Fe_2O_3$%) + (−1.610 × FeO%) + (2.720 × MnO%) + (0.881x MgO%) + (−0.907 × CaO%) + (−0.117 $Na_2O$%) + (−1.840 × $K_2O$%) + (7.244 × $P_2O_5$%).

### 7.4. Tectonic setting for the deposition of QPC and quartzite

Major oxides, trace elements and REE have been utilized extensively in the interpretation of tectonic setting for sediments and sedimentary rocks. Major elemental compositions have been used to discriminate different tectonic settings of sedimentary basins (Bhatia, 1983 and Roser and Korsch, 1986). Certain trace element ratios including REE were also used by different workers to decipher provenance study and tectonic setting of the sedimentary rocks (Taylor and McLennan, 1985; Cullers, 1994; Cullers, 2000; McLennan 1989; McLennan and Taylor, 1991). The major elemental geochemical parameters such as $Fe_2O_3$ + MgO%, $TiO_2$%, ($Al_2O_3$/$SiO_2$), ($K_2O/Na_2O$) and $Al_2O_3/(CaO + Na_2O)$ have been used to discriminate the plate tectonic setting of sedimentary basins.

Roser and Korsch (1988) used discriminant function analysis of major elements ($SiO_2$, $Al_2O_3$, total $Fe_2O_3$, MgO, CaO, $Na_2O$ and $K_2O$) in discriminating four different provenance groups. In $Fe_2O_3$ + MgO vs $TiO_2$ diagram, quartzite data show concentration around passive margin setting while QPC spread around passive margin setting and within active continental margin tectonic setting (Fig. 6A). Similarly, both QPC and quartzites occupy the position close to passive margin setting (Fig. 6B) in the $Fe_2O_3$ + MgO vs $Al_2O_3/SiO_2$ binary diagram of Bhatia (1983).

Immobile trace elements viz., La, Th, Sc and Zr are extremely useful in inferring the tectonic setting of sediments. On La-Th- Sc ternary diagram (Bhatia and Crook, 1986), the QPC and quartzites plot near passive margin and active continental margin fields (Fig. 7A). The QPC and quartzite samples occupy the Th-Zr/10 line close to passive margin setting and active continental margin (Bhatia and Crook, 1986) (Fig. 7B).

Majority of the QPC and quartzite samples plot in passive margin setting (Fig. 7C) in the $SiO_2$-$K_2O$ + $Na_2O$-$TiO_2$ + $Fe_2O_3$ (t) + MgO diagram (Kroonenberg, 1994). All the samples of QPC and quartzites occupy the field of passive margin tectonic setting (Fig. 7D) on $SiO_2$ vs $K_2O/Na_2O$ binary diagram of Roser and Korsch (1986). QPC and quartzite samples fall in passive margin setting as shown in Fig. 7E (Bhatia, 1983). Thus major and trace element data along with discriminant functions suggest passive margin tectonic setting for QPC- quartzites in the study area.

### 7.5. Th/U ratios in QPC and quartzites

Th/U in sedimentary rocks increases due to weathering and recycling and oxidation and removal of U. Although highly reduced sedimentary environments can have enriched U leading to low Th/U ratios. Weathering tends to result in oxidation of insoluble $U^{4+}$ to soluble $U^{6+}$ with loss of solution and elevation of Th/U ratios (McLennan et al., 1980, 1991). The Th/U ratio in most upper crustal rocks is typically range between 3.5 and 4.0 (McLennan et al., 1993). In sedimentary rocks, Th/U values higher than 4.0 may indicate intense weathering in source areas or sediment recycling. Upper crustal igneous rocks have Th/U averaging about 3.8, with considerable scatter (Taylor and McLennan 1985; Condie 1993). Th/U ratios in QPC and quartzites are below 4.0 (two samples of QPC show 4.0 to 9.0) are indicative of enrichment of uranium. In Th/U vs Th binary diagram, except two samples of QPC, all other samples of QPC and quartzites occupy the field below 4.0 ratio of Th/U (Fig. 7F) indicating uranium enrichment and reducing environment during the time of weathering and deposition of sediments. The presence of detrital grains of uraninite and pyrite in the QPC further support this observation (Kumar et al., 2012).

## 8. Discussion

Geochemical studies on QPC and quartzites exposed around western margin of Bonai Granite indicate their sub-arkosic to sub-lithic arenite composition which have undergone moderate to high degree of weathering as inferred from their CIA and PIA. This is also supported by petrographic observations which indicate the absence of any visible feldspar grains and low K, Na, Ca and Sr with high Rb/Sr ratio. Moderate to high weathering is also indicated by the oligomictic nature of QPC (Kumar et al., 2011a, 2012) and higher $SiO_2/Al_2O_3$ ratio in both QPC and quartzites. High $SiO_2$/ $Al_2O_3$ ratios indicate mature nature and probably indicate stable conditions of deposition. A-CN-K diagram indicate granite, minor granodiorite and tonalitic source rocks for both QPC and quartzites which might have been supplied by the Singhbhum Granite having similar composition exposed in the southern part of study area. A felsic and recycled source for these QPC- quartzites is also inferred by Th/Sc > 1.0 and Zr/Sc ratios > 10 which also indicate moderate weathering as well as reasonable enrichment of zircon during recycling processes of sediments.

Major as well as trace elements including immobile elements, critical ratios of major and trace elements together with rare earth elements also point mainly towards granitic source with some contribution from mafic–ultramafic rocks in the provenance. Ratios of $Al_2O_3/TiO_2$ and $SiO_2/MgO$ together with high average $SiO_2$ in QPC and quartzites along with low to moderate $Al_2O_3$ content in QPC and in quartzites suggest predominantly felsic source composition in the provenance. Trace element signatures such as high Th/Sc, La/Sc, Th/Cr and Zr/Sc ratio also support granitic provenance for QPC and quartzites. High REE and Th concentrations and low Sc (<1.0–4.0 ppm) indicates derivation of QPC from felsic igneous source rocks. Low Th and Sc in quartzites compared to QPC and variable Th/Sc ratio (0.23 to 13), suggest derivation of quartzites from felsic and minor mafic component in the provenance. Th/Sc vs Sc diagram strongly support that the QPC and quartzites in the study area were derived from felsic rocks relative to the mafic provenance. Enrichment of U, Th, Pb, La, Ce, Y in QPC are due to presence of uraninite, secondary uranyl minerals, adsorbed uranium associated with goethite, limonite, thorian uraninite and monazite whereas Cr, Cu and Ni are due to chromite, fuchsite, chalcopyrite and pyrite. Higher La/Sc and Th/Sc relative to the well-known Archean sediments suggest derivation from the fractionated and evolved crustal sources as well.

Geochemical diagrams based on least mobile elements like La, Th and Sc and $TiO_2$ vs. Ni mainly suggestive of felsic and minor mafic provenance (Condie, 1993 and Floyd et al., 1989). High Cr/Th ratios in QPC (2.02–25) and quartzites (6.88–94) indicate presence of ultramafic rocks in the provenance whereas low to moderate ratio of Y/Ni in QPC (0.36–12.4) and quartzites (0.29–1.88) point some contribution of mafic rocks from the source region. Thus presence of Th, U, high Th/Sc, La/Sc ratios together with elevated concentrations of Cr, Cr/Th, Cr/Zr and presence of chromite in QPC matrix indicates granite-greenstone provenance for QPC-quartzites. Hence mixed provenance is suggested for QPC- quartzite in the study area. Based on geochemical study from Keonjhar area, Singhbhum-Orissa Craton, Ghosh et al. (2016) also suggested a mixed signature of source rocks from greenstone to differentiated post-Archean UCC types.

REE patterns of QPC and quartzites are comparable to the REE patterns of Singhbhum Granite and Bonai Granite that suggest their derivation from some of the phases of SBG and BG. Felsic provenance is also supported by high LREE/HREE ratios and negative Eu anomaly in both QPC and quartzites. Most of the QPC and quartzite samples from study area show contrast with those noted in Archean greenstone belts, which display REE patterns similar to typical post-Archean shales and provides evidence for the presence of a Mesoarchean differentiated continental crust in the Singhbhum region. Differential signature of crust has also been inferred from the Mesoarchean Keonjhar Quartzite by Ghosh et al. (2016). The present data set from the western part of the craton also

**Table 8**
Comparison of geological environment of radioactive QPCs from western margin of Archean Singhbhum-Orissa Craton vis-a-vis important radioactive QPCs from Canadian, South African, Southern and Eastern Indian Cratons.

| Geological/sedimentological/ mineralogical characteristics/economic parameters | Study area (Kumar et al., 2012) | Elliot Lake, Canada (Schidlowski, 1975; Nedachi et al., 2005 | Witwatersrand, South Africa (Feather and Glatthaar, 1987) | Jacobina, Brazil (Milesi et al., 2002) | Dharwar Craton, Southern India (Varma et al., 1988) | Daitari Basin, Eastern India (Mukhopadhyay et al., 2016; Kumar et al., 2011) |
|---|---|---|---|---|---|---|
| Age (Ma) | 3300–2800 | 2500–2160 | 2800–2300 | 2500–2200 | 2900–2600 | 3440–3100 |
| Clast | White vein qtz, smoky qtz chert, quartzite | White vein qtz, chert, quartzite | White vein qtz, chert, quartzite | Qtz | White vein qtz, chert, quartzite | White vein qtz, chert, quartzite |
| Matrix | Qtz, Ser, Chl, Py | Qtz, Fsp, Ser, Py | Qtz, Ser, Chl, Py | Qtz, Py | Qtz, Ser, Chl, Py, Mc | Ser, Chl |
| Heavies | Mag, Zrn, Ilm, Chr, Rt, Tur, Py, Ccp, Mnz | Ilm, Chr, Mag, Zrn, Grt, Rt, Tur, Ap | Zrn, Chl, Rt | Zrn, Py, Rt, Thr, Mnz, Chr | Rt, Grt, Zrn, Ilm, Ep | Py, Urn, Zrn, Ccp, Mnz, Chr, Rt |
| U-Minerals | Urn, uranophane | Urn, brannerite, thucholite, Aln, uranothorite, coffinite | Urn, brannerite, thucholite, coffinite, uranothorite, leucoxene | Urn, brannerite, pitchblende | Urn, brannerite, pitchblende | Urn, coffinite, altered U–Th and U–Ti phases |
| Associated ore minerals | Py | Xtm | Py, Apy, Po, Gn, Au, platinoids, cobaltite | Au | Py, Apy, Po, Gn, Ccp, Mrc, Sp, Mo | Py, Ccp |
| Grade $U_3O_8$ | <0.01–0.039% | 0.12% | 0.03% | 0.10% | 0.047–0.051% | <0.01–0.03% |
| Au | 30 ppb–1.52 ppm | 0.2–1.2 ppm | 10–12 ppm | 10 ppm | Upto 1.5 ppm | – |
| *Uraninite composition of QPC matrix* | | | | | | |
| $UO_2$ | 63.86–71.13 | 58.0–69.0 | 61.1–72.5 | – | 45.32–54.70 | 57.26–75.45 |
| $ThO_2$ | 5.48–6.42 | 4.0–9.0 | 1.4–10.2 | – | 8.24–10.74 | 4.10–11.71 |
| PbO | 10.57–12.59 | 18 | 14.7–30.3 | – | 6.54–18.76 | 6.80–15.07 |
| $REE_2O_3$ | 1.57–2.23 | 3.0–8.0 | – | – | – | 9.49 |
| $UO_2/ThO_2$ | 10.30–12.38 | 9.23 | 6.4–47.4 | – | 4.67–5.43 | 0.98–2.98 |

Mineral Abbreviations (after Kretz, 1983): Qtz-Quartz, Ser-Sericite, Chl-Chlorite, Rt-Rutile, Zrn-Zircon, Chr-Chromite, Ilm-Ilmenite, Mag-Magnetite, Tur-Tourmaline, Ap-Apatite, Grt-Garnet, Ep-Epidote, Fsp-Felspar, Mc-Microcline, Mnz-Monazite, Urn- Uraninite, Thr-Thorite, Py-Pyrite, Apy-Arsenopyrite, Po-Pyrhhotite, Gn-Galena, Ccp-Chalcopyrite, Mrc-Marcasite, Sp-Sphalerite, Mo-Molybdenite, Aln- Allanite, Xtm- Xenotime, Au-Gold.

corroborates this idea. The study area QPC and quartzites could have been formed in the passive margin tectonic setting as indicated by their geochemical signatures. Thus present study and the study by Ghosh et al. (2016) cover the Paleo-Mesoarchean upper crust of the Singhbhum-Bonai Craton strengthen the database in support of a modern style geodynamic setting comprehensively from a rarely preserved succession of early Archean.

The low Th/U ratio (<4.0) in QPC and quartzites indicates enrichment of uranium and manifestation of reducing environment during the time of deposition of sediments. The presence of detrital grains of uraninite and pyrite (Kumar et al. 2012) further support this observation in the QPC. Low Th/U ratios suggest a relative enrichment of uranium and further indicative of K-rich granites in provenance (Taylor and Mclennan, 1985). Similar observations have also been inferred by Mukhopadhyay et al. (2016) while studying nature and source of detrital uraninite from Mahagiri siliciclastics from Daitari-Tomka basin of Singhbhum Craton.

Since pyrite and uraninite are highly unstable mineral phases in the present day oxidizing conditions or present atmospheric conditions, preservation of these two minerals as discrete grains in Archean QPC signify the stability of these minerals. QPCs have undergone moderate to high degree of chemical weathering either in the source area or during the deposition or at the site of deposition. Preservation of uraninite and pyrite in Archean QPC under these weathering conditions signify strong evidence for the presence of low oxygen levels in the atmosphere (Maynard et al., 1991) during formation of QPC-quartzites at least in parts of eastern India Craton.

The whole rock and mineral chemical signatures of the study area are well comparable with that of established QPC hosted U belts from South Africa (Witwatersrand), Canada (Elliot Lake) and southern India (Dharwar Craton) (Table 8). The QPC from western part of SOC has resemblance with other major deposits from worldwide, thus indicating near similar conditions of formation of the uraninite and environment of deposition.

## 9. Conclusions

Geochemical signatures of QPC and quartzites indicate that they have undergone moderate to high degree of chemical weathering. CIA study also suggest that granite, granodioritic and tonalitic rocks representing the source provenance which upon weathering and transportation provided the detritus to the supra-crustal units in the form of QPC and quartzites. Major, trace elements and REE data suggest that these sediments have been largely derived from felsic igneous rocks viz., Singhbhum Granite and Bonai Granite with minor contribution from mafic and ultramafic sources. Source criteria have also been confirmed by their trace elemental signatures viz., high Th, U, La, Ce, high critical elemental ratios of Th/Sc, La/Sc, Zr/Sc and high Cr, Cr/Th. Thus geochemical data indicate mixed provenance for QPC and quartzite. Geochemical studies further suggest that QPC-quartzite sequence have been deposited in a passive margin tectonic setting developed during Archean (3.3 to 2.8 Ga) along western margin of Bonai Granite substantiated by their high $SiO_2/Al_2O_3$ ratios, LREE enrichment, high Th/Sc, La/Sc and high Rb/Sr ratios.

Comparison of QPC of the study area show similarity in mineralogical composition, whole rock chemistry and uraninite chemistry of QPCs from Canada, South Africa and Southern India. The Archean–Paleoproterozoic QPC world over are considered good targets for moderate to high tonnage and low grade (0.03–0.1% $U_3O_8$) uranium deposits because they contain detrital uraninite and gold primarily as a products of liberation and transportation from Archean granite-greenstone terranes. QPC– quartzite

sequence contains 30 ppb to 1.5 ppm Au, 62 to 1245 ppm REE and < 10 to 692 ppb of Pt. Detailed field, mineralogical and geochemical characteristics of QPC and quartzites bears similarity with other U bearing Mesoarchean QPCs. Hence can be targeted for detailed investigations to further explore the study area and the analogous areas to develop into a major U (± Au-REE-PGE) province.

## Acknowledgements

The authors are thankful to the Director, Atomic Minerals Directorate for Exploration and Research (AMD) for according necessary permission to publish this paper. Prof. Franco Pirajno and Prof. M Santosh are thanked for their critical editorial handling of the paper and for constructive suggestions. Sincere thanks are also due to the reviewers of OGR for their fruitful suggestions in improving the quality of the research paper. We also thank Dr. P R Sahoo, Mr. Rahul Mukherjee, IIT (ISM) Dhanbad and Mr. E. Lingamurty, AMD, Nagpur for their help to organize the manuscript and drafting some of the illustrations. The research paper is part of the Ph.D. work of AK carried out at IIT(ISM), Dhanbad and AMD, Jamshedpur. ASV is thankful to the DST-FIST funding to the Department of Applied Geology, IIT(ISM), Dhanbad.

## References

Akarish, A.I.M., EL-Gohary, A.M., 2011. Provenance and source area weathering derived from the geochemistry of Pre-Cenomanian sandstones, east Sinai. Egypt J. Appl. Sci. 11 (17), 3070–3088.
Bandyopadhyay, P.K., Chakrabarti, A.K., Deomurari, M.P., Misra, S., 2001. 2.8 Ga old Anorogenic granite-acid volcanic association from western margin of Singhbhum-Orissa craton, eastern India. Gond. Res. 4, 465–475.
Basu, A.R., Bandyopadhyay, P.K., Chakraborti, R., Zou, H., 2008. Large 3.4 Ga algoma type BIF in the Eastern Indian Craton. Goldschmidt Conference 2008, Vancouver (Canada), Abstract Volume. Geochim. Cosmochim. Acta 72 (12S), A59.
Bergen, L., Fayek, M., 2012. Petrography and geochronology of the Pele Mountain quartz pebble conglomerate uranium deposit, Elliot Lake District. Canada Am. Mineral. 97, 1274–1283.
Bhatia, M.R., 1983. Plate tectonics and geochemical composition of sandstones. J. Geol. 91, 611–627.
Bhatia, M.R., Crook, K.A.W., 1986. Trace elements characteristics of greywackes and tectonic setting discrimination of sedimentary basins. Contrib. Mineral. Petrol. 92, 181–193.
Bhushan, S.K., Sahoo, P., 2010. Geochemistry of clastic sediments from Sargur Supracrustals and Bababudan Group, Karnataka: Implications on Archean-Proterozoic Boundary. J. Geol. Soc. India 75, 829–840.
Chakrabarti, G., Shome, D., Bauluz, B., Sinha, S., 2009. Provenance and weathering history of mesoproterozoic clastic sedimentary rocks from the Basal Gulcheru Formation, Cuddapah Basin, India. J. Geol. Soc. India 74, 119–130.
Chakrabarti, K., Ecka, N.R.R., Mishra, B., Ramesh Babu, P.V., Parihar, P.S., 2011. Paleoproterozoic Quartz-Pebble Conglomerate type uranium mineralisation in Mankarhachua area, Angul district, Orissa. J. Geol. Soc. India 77, 443–449.
Cingolani, C.A., Manassero, M., Abre, P., 2003. Composition, provenance and tectonic setting of Ordovician siliciclastic rocks in the San Rafael block: Southern extension of the Precordillera crustal fragment, Argentina. J. South Am. Earth Sci. 16, 91–106.
Condie, K.C., 1993. Chemical composition and evolution of the upper continental crust. Contrasting results from surface samples and shales. Chem. Geol. 104, 1–37.
Cox, R., Lowe, D.R., Cullers, R.L., 1995. The influence of sediment recycling and basement composition on evolution of mudrock chemistry in the southwestern United States. Geochim. Cosmochim. Acta 59 (14), 2919–2940.
Cullers, R.L., 1994. The controls on the major and trace element variation of shales, siltstone and sandstones of Pennsylvanian-Permian age from uplifted continental blocks in Colorado to platform sediment in Kansas, USA. Geochim. Cosmochim. Acta 58, 4955–4972.
Cullers, R.L., 2000. Geochemistry of the Mesoproterozoic Lakhanda shales in southeastern Yakutia, Russia: implications for mineralogical and provenance control, and recycling. Precamb. Res. 104, 77–93.
Cullers, R.L., Graf, J., 1983. Rare earth elements in igneous rocks of the continental crust: intermediate and silicic rocks, ore petrogenesis. In: Henderson, P. (Ed.), Rare earth Geochemistry. Elsevier, Amsterdam, pp. 275–312.
Dahlkamp, F.J., 1993. Uranium Ore Deposits. Springer-Verlag. 460p.
Dankert, B.T., Hein, A.A..Kim., 2010. Evaluating the structural character and tectonic history of the Witwatersrand Basin. Precamb. Res. 177, 1–22.
Das, A.K., Awati, A.B., Sahoo, P., 1988. Quartz-pebble conglomerates of the Singhbhum Craton, Bihar and Orissa. Mem. Geol. Soc. India 9, 83–87.
Feather, C.E., Glatthaar, C.W., 1987. A review of uranium-bearing minerals in the Dominion and Witwatersrand placers. In: Pretorius, A. (Ed.), Uranium Deposits in Proterozoic Quartz-Pebble Conglomerates, Technical Report (D. International Atomic Energy Agency, Vienna, pp. 355–386.
Fedo, C.M., Nesbitt, H.W., Young, G.M., 1995. Unravelling the effects of potassium metasomatism in sedimentary rocks and paleosols with implications for paleoweathering conditions and provenance. Geology 23, 921–924.
Floyd, P.A., Winchester, J.A., Park, R.G., 1989. Geochemistry and tectonic setting of Lewisian clastic metasediments from early Proterozoic Loch Maree Group of Gairloch, N.W, Scotland. Precamb. Res. 45, 203–214.
Frimmel, H.E., 2005. Archean atmospheric evolution: evidence from the Witwatersrand gold fields, South Africa. Earth Sci. Rev. 70, 1–46.
Frimmel, H.E., Minter, W.E.L., 2002. Recent developments concerning the geological history and genesis of the Witwatersrand gold deposits, South Africa. Soc. Econ. Geol., 17–45 Special Publication no. 9.
Ghosh, S., De, S., Mukhopadhyay, J., 2016. Provenance of >2.8 Ga Keonjhar Quartzite, Singhbhum Craton, Eastern India: Implications for the Nature of Mesoarchean Upper Crust and Geodynamics. J. Geol. 124 (3), 331–351.
Grandstaff, D.E., 1980. Origin of uraniferous conglomerates at Elliot Lake, Canada and Witwatersrand, South Africa: implications for oxygen in the Precambrian Atmosphere. Precamb. Res. 13, 1–26.
Grandstaff, D.E., 1981. Microprobe analyses of uranium and thorium in uraninite from the Witwatersrand, South Africa and Blind River, Ontario, Canada. In Genesis of uranium and gold bearing Precambrian Quartz- pebble conglomerates. In: Proceedings of a Workshop, October 13–15, Golden, Colorado; Geol. Sur. Prof. Paper 1161-A-BB, J1–J5.
Haque, M.W., Dutta, S.K., Sinha, P.K., 2001. Dhanjori quartz-pebble conglomerate: a new prospects for rare earth elements. In: Singh, S.P. (Ed.), Precambrian Crustal Evolution and Mineralization (PCEM) in India. South Asian Association of Economic Geology, Patna, pp. 315–322. Chapter.
Hazen, R.M., Ewing, R.C., Sverjensky, D.A., 2009. Evolution of uranium and thorium minerals. Ameri. Mineral. 94, 1293–1311.
Heron, M.M., 1988. Geochemical classification of terrigenous sands and shales from core and log data. J. Sediment Petrol. 58, 820–829.
Holland, H.D., 1984. The Chemical Evolution of the Atmosphere and the Oceans. Princeton, New Jersey. John Wiley, New York. 389.
IAEA, 1996. World distribution of uranium deposits. A guide book to accompany IAEA map, Vienna, 223.
Jacobson, A.D., Blum, J.D., Chamberlian, C.P., Craw, D., Koons, P.O., 2003. Climate and tectonic controls on chemical weathering in the New Zealand Southern Alps. Geochim. Cosmochim. Acta 37, 29–46.
Kretz, 1983. Symbols for rock-forming minerals. Am. Mineral. 68, 277–279.
Kroonenberg, S.B., 1994. Effects of provenance, sorting and weathering on the geochemistry of fluvial sands from different tectonic and climatic environments: Proceedings of the 29th Int. Geol. Cong., Part A, 69–81.
Kumar, A., 2013. Geological, petrological and geochemical characterization of radioactive quartz pebble conglomerates (QPC) along western margin of Bonai Granite, Sundergarh District, Orissa. Unpub. Ph.D. thesis, ISM, Dhanbad, India. 377.
Kumar, A., Pande, D., 2005. Annual report for field season, 2005-06, QPC Investigations, Unpub. Rept. AMD, DAE, Hyderabad.
Kumar, A., Birua, S.N.S., Pande, D., Nath, A.R., Ramesh Babu, P.V., Pandit, S.A., 2009. Radioactive quartz-pebble conglomerates from western margin of Bonai Granite pluton, Sundargarh district, Orissa – a new find. J. Geol. Soc. India 73, 537–542.
Kumar, A., Mishra, B., Chakrabarti, K., Ecka, N.R.R., Ramesh Babu, P.V., Parihar, P.S., 2011a. Petrographic and geochemical characterization of quartz-pebble conglomerates from Koira and Daitari basins of Orissa. Indian Mineralogist, Mineralogical Soc. India Mysore, Golden Jubilee volume, 45, 1, 9–23.
Kumar, A., Venkatesh, A.S., Ramesh Babu, P.V., Nandakishore, S., 2011b. A Note on the presence of Au-REE ± Ag–Pt in uraniferous Archean Iron Ore Group sediments, Western margin of Bonai Granite pluton, Eastern India. J. Explor. and Res. Atom. Min. (EARFAM), 21, 9–21, AMD, DAE, Hyderabad.
Kumar, A., Venkatesh, A.S., Ramesh Babu, P.V., Nayak, S., 2012. Genetic implications of rare uraninite and pyrite in quartz-pebble conglomerates from Sundargarh district of Orissa, Eastern India. J. Geol. Soc. India 79 (3), 279–286.
Lichte, F., Meier, A.L., Crock, J.G., 1987. Determination of Rare-earth elements in geological materials by ICPMS. Anal. Chem 59 (8), 1150–1157.
Mahadevan, T.M., 2002. Geology of Bihar and Jharkhand, In (Ed.) Geol. Soc. India, pp. 564.
Mahalik, N.K., 1987. Geology of rocks lying between Gangpur Group and Iron ore Group of the Horse Shoe Syncline in North Orissa, India. J. Earth Sci. 14, 73–83.
Maynard, J.B., Ritzer, S.D., Sutton, S.J., 1991. Chemistry of sands from the modern Indus River and the Archean Witwatersrand basin: Implications for the composition of the Archean atmosphere. J. Geol. 19, 265–268.
McDonough, W.F., Sun, S.S., 1995. The composition of the earth. Chem. Geol. 120, 223–253.
McLennan, S.M., 1989. Rare earth elements in sedimentary rocks- Influence of provenance and sedimentary processes. Rev. Min. 21, 169–200.
McLennan, S.M., 2001. Relationships between the trace element composition of sedimentary rocks and upper continental crust. Geochem. Geophys. Geosyst. 2 (4), 1021–1024.
McLennan, S.M., Taylor, S.R., 1991. Sedimentary rocks and crustal evolution: Tectonic setting and secular trends. J. Geol. 99, 1–21.
McLennan, S.M., Nance, W.B., Taylor, S.R., 1980. Rare earth element-thorium correlations in the sedimentary rocks, and the composition of the continental crust. Geochim. Cosmochim. Acta 44, 1833–1839.

McLennan, S.M., Hemming, S., McDaniel, D.K., Hanson, G.N., 1993. Geochemical approaches to sedimentation, provenance and tectonics. In Processes controlling the composition of clastic sediments (Johnsson, M. J. and Basu, A, edited). Geol. Soc. Amer. Special paper 284, 21–40.

Milesi, J.P., Ledru, P., Marcoux, E., Mougeot, R., Johan, V., Lerouge, C., Sabaté, P., Bailly, L., Respaut, J.P., Skipwith, P., 2002. The Jacobina Paleoproterozoic gold-bearing conglomerates, Bahia, Brazil: a "hydrothermal shear-reservoir" model. Ore Geol. Rev. 19, 95-136

Mishra, K.S., Durairaju, S., Rajasekharan, P., Das, A.K., 1997. Occurrence of U-Au-REE bearing quartz-pebble conglomerate at Sayamba - Taldih, Sundargarh district, Orissa. J. Geol. Soc. India 50, 93–94.

Mishra, B., Pande, D., Gogoi, J., Kumar, A., Ramesh Babu, P.V., Parihar, P.S., 2008. Quartz-Pebble Conglomerate Type Uranium Mineralization in Balia-Rankia Area of Daitari-Tomka basin, Jaipur district, Orissa. J. Explor. Res. Atoms. Min. 18, 1–14.

Mukhopadhyay, J., Beukes, N.J., Armstrong, R.A., Zimmermann, U., Ghosh, G., Medda, R.A., 2008. Dating the oldest greenstone in India: a 3.51 Ga precise U-Pb SHRIMP Zircon Age for Dacitic Lava of the Southern Iron Ore Group, Singhbhum Craton. J. Geol. 116, 449–461.

Mukhopadhyay, J., Crowley, Q., Ghosh, S., Ghosh, G., Chakrabarti, K., Misra, B., Bose, S., 2014. Oxygenation of the Archean atmosphere: new paleosol constraints from eastern India. Geology 42, 923–926.

Mukhopadhyay, J., Mishra, B., Chakrabarti, K., De, S., Ghosh, G., 2016. Uraniferous paleoplacers of the Mesoarchean Mahagiri quartzite, Singhbhum craton, India: Depositional controls, nature and source of >3.0 Ga detrital uraninites. Ore Geol. Rev. 72, 1290–1306.

Nagarajan, R., Armstrong-Altrin, J.S., Nagendra, R., Madhavaraju, J., Moutte, J., 2007. Petrography and geochemistry of terriginous sedimentary rocks in the Neoprotrozoic Rabanpalli Formation, Bhima Basin, Southern India: Implications for Paleoweathering conditions, Provenance and source rock composition. J. Geol. Soc. India 70, 297–312.

Nedachi, Y., Nedachi, M., Bennett, G., Ohmoto, H., 2005. Geochemistry and mineralogy of the 2.45 Ga Pronto paleosols. Ontario. Canada. Chem. Geol. 214, 21–44.

Nesbitt, H.W., Young, G.M., 1982. Early Proterozoic climates and plate motions inferred from major element chemistry of lutites. Nature 199, 715–717.

Nesbitt, H.W., Young, G.M., 1984. Prediction of some weathering trends of plutonic and volcanic rocks based on thermodynamic and kinetic considerations. Geochim. Cosmochim. Acta 48, 1523–1534.

Nesbitt, H.W., McLennan, S.M., Keays, R.R., 1996. Effects of chemical weathering and sorting on the petrogenesis of siliciclastic sediments with implications for provenance studies. J. Geol. 104, 525–542.

Oguri, K., Shimoda, G., Tatsumi, Y., 1999. Quantitative determination of Au and PGEs in geological sample using improved NiS fire assay and tellurium precipitation with ICP-MS. Chem. Geol. 157, 189–197.

Pandit, S.A., 2002. Uranium occurrences in the quartz-pebble conglomerate in Karnataka. Expl. Res. Atom. Min., AMD, Hyderabad, 14, 131-146.

Parihar, P.S., 2012. Resurgent India – Vision 2020 in Metals and Minerals Sector, September 28, 2012, New Delhi.

Pettijohn, F.J., Potter, P.E., Siever, R., 1972. Sand and Sandstones. Springer-verlag, New York, p. 619.

Phillips, G.N., Law, J.D.M., 2000. Witwatersrand gold fields: geology, genesis, and exploration. Soc. Econ. Geol. Rev. 13, 439–500.

Rama Rao, B.V., 1974. Discovery of uraniferous Precambrian conglomerates at Chikmagalur, Karnataka state. Curr. Sci. 44, 174–175.

Red Book, 2011. Uranium: Resources, Production and Demand. Joint report by NEA and IAEA, ISBN 978-92-64-17803-8; 489p.

Robertson, D.S., 1962. Thorium and uranium in Blind River ores. Econ. Geol. 57, 1175–1184.

Robinson, A., Spooner, E.T.C., 1982. Source of the detrital components of uraniferous conglomerates, Quirke ore zone, Elliot Lake, Ontario, Canada. Nature 299, 622–624.

Roser, B.P., Korsch, R.J., 1986. Determination of tectonic setting of sandstone-mudstone suites using $SiO_2$ content and $K_2O/Na_2O$ ratio. J. Geol. 94, 635–650.

Roser, B.P., Korsch, R.J., 1988. Provenance signatures of sandstone- mudstone suites determined using discriminant functions analysis of major element data. Chem. Geol. 67, 119–139.

Saager, R., Stupp, H.D., 1983. U-Ti phases from Precambrian Quartz-pebble conglomerates of the Elliot Lake area, Canada and the Pongoloa Basin, South Africa. TMPM Tschermaks Min. Petr. Mitt, Federal Repub. German, 32, 83-102.

Saha, A.K., 1994. Crustal evolution of Singhbhum- North Orissa Region, Eastern India. Mem. Geol. Soc. India 27, 341.

Sahoo, P.R., Venkatesh, A.S., 2015. Constraints of mineralogical characterization of gold ore: Implication for genesis, controls and evolution of gold from Kundarkocha gold deposit, eastern India. J. Asian Earth Sci. 97, 136–149.

Sarkar, S.N., Saha, A.K., 1992. Aerial photo-interpretation and ground check of the Bonai granitic complex and the associated supracrustals. India. J. Geol. 64 (2), 223–233.

Schidlowski, M., 1975. Uraniferous constituents of the Witwatersrand conglomerates: Ore microscopic observations and implications for the Witwatersrand metallogeny. In: genesis of uranium and gold bearing Precambrian quartz-pebble conglomerates, USGS Prof. Paper, 1161-A-BB, N1–N24.

Sengupta, S., Paul, D.K., De Laeter, J.R., McNaughton, N.J., Banddyopadhyay, P.K., De Smeth, J.B., 1991. Mid- Archaean evolution of the Eastern Indian Craton: geochemical and isotope evidence from the Bonai Granite pluton. Precamb. Res. 49, 23–37.

Sengupta, S., Corfu, F., McNutt, H.R., Paul, D.K., 1996. Mesoarchaean crustal history of the eastern Indian Craton: Sm-Nd and U-Pb isotopic evidence. Precamb. Res. 77, 17–22.

Singh, P., Rajamani, V., 2001. Geochemistry of the flood plain sediments of the Kaveri river, southern India. J. Sed. Res. 71, 50–60.

Smith, N.D., Minter, W.E.L., 1980. Sedimentalogical controls of gold and uranium in two Witwatersrand palaeo-placers. Econ. Geol. 75 (1), 1–14.

Taylor, S.R., McLennan, S.M., 1985. The continental Crust: Its composition and evolution. Blackwell, 311.

Uvarova, Y.A., Kyser, T.K., Geagea, M.L., Chipley, D., 2014. Variations in the uranium isotopic compositions of uranium ores from different types of uranium deposits. Geochim. Cosmochim. Acta 146, 1–17.

Varma, H.M., Dhana Raju, R., Raju, B.N.V., Narayan Das, G.R., 1988a. Mineragraphy of uranium ore from Dabguli-Arbail area, North Kanara District, Karnataka and its genetic significance. Mem. Geol. Soc. India 9, 55–63.

Varma, H.M., Dhana Raju, R., Raju, B.N.V., Bhanumurthy, K., Mahadevan, T.M., 1988b. Preliminary electron microprobe study of uranium, thorium and lead distribution in some U-Th minerals from various parts of India. Mem. Geol. Soc. India 9, 115–128.

Vasudeva Rao, M., Sinha, K.K., Mishra, B., Balachandran, K., Srinivasan, S., Rajasekharan, P., 1988. Quartz-pebble conglomerate from the Dhanjori-Singhbhum uranium Province. Mem. Geol. Soc. India 9, 89–95.

Viswanath, R.V., Roy, M.K., Pandit, S.A., Narayan Das, G.R., 1988. Uranium mineralization in the Quartz- Pebble Conglomerates of Dharwar Supergroup, Karnataka. Mem. Geol. Soc. India 9, 33–41.

Wronkiewicz, D.J., Condie, K.C., 1987. Geochemistry of archean shales from the witwatersrand supergroup, South Africa: source area weathering and provenance. Geochim. Cosmochim. Acta 54, 2401–2416.

Wronkiewicz, D.J., Condie, K.C., 1989. Geochemistry and provenance of sediments from the Pongola Supergroup, South Africa: Evidence for a 3.0 Ga old continental craton. Geochim. Cosmochim. Acta 53, 1537–1549.

Yan, X.P., Kerrich, R., Hendry, M.J., 2000. Trace element geochemistry of a thick till and clay rich aquitard sequence, Saskatchewan, Canada. Chem. Geol. 164, 93–120.